JOURNAL OF PETROLOGY | VOLUME 47 | NUMBER 3 | PAGES 505–539 | 2006 | doi:10.1093/petrology/egi084

The Genesis of Intermediate and Silicic Magmas in Deep Crustal Hot Zones

C. ANNEN[1]*, J. D. BLUNDY[2] AND R. S. J. SPARKS[2]

[1]SECTION DES SCIENCES DE LA TERRE, UNIVERSITÉ DE GENÈVE, 13 RUE DES MARAÎCHERS, 1205 GENÈVE, SWITZERLAND

[2]DEPARTMENT OF EARTH SCIENCES, UNIVERSITY OF BRISTOL, WILLS MEMORIAL BUILDING, BRISTOL BS8 1RJ, UK

RECEIVED APRIL 14, 2005; ACCEPTED OCTOBER 17, 2005
ADVANCE ACCESS PUBLICATION DECEMBER 7, 2005

A model for the generation of intermediate and silicic igneous rocks is presented, based on experimental data and numerical modelling. The model is directed at subduction-related magmatism, but has general applicability to magmas generated in other plate tectonic settings, including continental rift zones. In the model mantle-derived hydrous basalts emplaced as a succession of sills into the lower crust generate a deep crustal hot zone. Numerical modelling of the hot zone shows that melts are generated from two distinct sources; partial crystallization of basalt sills to produce residual H_2O-rich melts; and partial melting of pre-existing crustal rocks. Incubation times between the injection of the first sill and generation of residual melts from basalt crystallization are controlled by the initial geotherm, the magma input rate and the emplacement depth. After this incubation period, the melt fraction and composition of residual melts are controlled by the temperature of the crust into which the basalt is intruded. Heat and H_2O transfer from the crystallizing basalt promote partial melting of the surrounding crust, which can include meta-sedimentary and meta-igneous basement rocks and earlier basalt intrusions. Mixing of residual and crustal partial melts leads to diversity in isotope and trace element chemistry. Hot zone melts are H_2O-rich. Consequently, they have low viscosity and density, and can readily detach from their source and ascend rapidly. In the case of adiabatic ascent the magma attains a super-liquidus state, because of the relative slopes of the adiabat and the liquidus. This leads to resorption of any entrained crystals or country rock xenoliths. Crystallization begins only when the ascending magma intersects its H_2O-saturated liquidus at shallow depths. Decompression and degassing are the driving forces behind crystallization, which takes place at shallow depth on timescales of decades or less. Degassing and crystallization at shallow depth lead to large increases in viscosity and stalling of the magma to form volcano-feeding magma chambers and shallow plutons. It is proposed that chemical diversity in arc magmas is largely acquired in the lower crust, whereas textural diversity is related to shallow-level crystallization.

KEY WORDS: *magma genesis; deep hot zone; residual melt; partial melt; adiabatic ascent*

INTRODUCTION

A key question in igneous petrology concerns the origin of intermediate to silicic magmatic rocks, such as voluminous Cordilleran granite batholiths (diorites, tonalites, granodiorites and granites) and the evolved volcanic rocks (andesites, dacites and rhyolites) of destructive plate margins. The continental crust has an estimated silicic andesite to dacite composition, with a vertical stratification from mafic lower crust to more evolved granite-dominated upper crust (Rudnick & Fountain, 1995). The origin of intermediate to silicic igneous rocks is, therefore, central to understanding the evolution of the continental crust.

In subduction settings melt is generated by partial melting in the mantle wedge where primary mafic magmas form by some combination of addition of H_2O-rich fluids or melts released from the subducted slab (e.g. Davies & Stevenson, 1992; Tatsumi & Eggins, 1995; Schmidt & Poli, 1998; Ulmer, 2001; Grove *et al.*, 2002; Forneris & Holloway, 2003) and mantle decompression resulting from subduction-induced corner flow (e.g. Sisson & Bronto, 1998; Elkins-Tanton *et al.*, 2001; Hasegawa & Nakajima, 2004). Experimental studies of mantle melting (e.g. Ulmer, 2001; Parman & Grove, 2004; Wood, 2004),

*Corresponding author. Telephone: ++41 22 379 66 23. Fax: ++41 22 379 32 10. E-mail: Catherine.Annen@terre.unige.ch

and observations of the petrology and geochemistry of mafic arc magmas, indicate that primary, mantle-derived magmas range in composition from basalts to magnesian andesites (Tatsumi, 1982; Tatsumi & Eggins, 1995; Bacon *et al.*, 1997; Conrey *et al.*, 1997; Carmichael, 2002, 2004; Grove *et al.*, 2002). In terms of liquidus temperatures and dissolved H_2O contents there is a range from dry and hot magmas to wet and cool varieties, even within a single volcanic arc (e.g. Sisson & Layne, 1993; Baker *et al.*, 1994; Elkins-Tanton *et al.*, 2001; Pichavant *et al.*, 2002*a*). Volcanic rocks with MgO-rich compositions that could be in equilibrium with the mantle wedge are rare in continental arcs and only a minor component of island arcs, an observation attributable to density filtering and intracrustal 'processing' of ascending magmas. This processing accounts for the predominance of evolved (silica-rich) volcanic rocks and granitic plutonic rocks in continental and mature island arcs.

The generation of intermediate and silicic arc magmas is widely attributed to two main processes: differentiation of primary magmas by crystallization within the crust or uppermost mantle (e.g. Gill, 1981; Grove & Kinzler, 1986; Musselwhite *et al.*, 1989; Rogers & Hawkesworth, 1989; Müntener *et al.*, 2001; Grove *et al.*, 2002, 2003) and partial melting of older crustal rocks (e.g. Smith & Leeman, 1987; Atherton & Petford, 1993; Tepper *et al.*, 1993; Rapp & Watson, 1995; Petford & Atherton, 1996; Chappell & White, 2001; Izebekov *et al.*, 2004). These processes can occur simultaneously with the heat and volatiles (principally H_2O) liberated from the primary magmas triggering crustal melting (Petford & Gallagher, 2001; Annen & Sparks, 2002). Additionally crustal rocks can be assimilated into mantle-derived magmas (DePaolo, 1981). The assimilated components may be much older than, and petrogenetically unrelated to, the arc magmas and possess distinctive trace element and isotope geochemistry. Partial melting can also occur in igneous rocks, including cumulates, that have formed from earlier arc magmas; in this case the assimilated components and arc magmas may have strong geochemical affinities (e.g. Heath *et al.*, 1998; Dungan & Davidson, 2004). Evidence for crustal assimilation and mixing of melts and crystals from different sources is common (Grove *et al.*, 1988, 1997; Musselwhite *et al.*, 1989; De Paolo *et al.*, 1992). These processes are central to models of assimilation and fractional crystallization (AFC; DePaolo, 1981) and mixing, assimilation, storage and hybridization (MASH; Hildreth & Moorbath, 1988).

A key question is at what depth chemical differentiation occurs. Although the existence of shallow sub-volcanic magma chambers is indisputable, based on geophysical evidence as well as petrological and geological observations, it is less clear that such chambers are the place where most chemical differentiation takes place. To produce igneous rocks that contain more than 60 wt % SiO_2 by fractional crystallization, 60% or more crystallization of a typical primitive arc basalt is required (e.g. Foden & Green, 1992; Müntener *et al.*, 2001). The volume of parental mafic magma that crystallizes is, therefore, typically twice as much as the evolved magma produced. As large granitoid batholiths and voluminous eruptions involve hundreds to thousands of km^3 of silicic magma (e.g. Smith, 1979; Crisp, 1984; Bachmann *et al.*, 2002), huge volumes of associated mafic cumulates are required. However, geological and geophysical evidence for the requisite large volumes of complementary dense mafic cumulates in the shallow crust is generally lacking. One resolution to this problem is density-driven sinking of mafic cumulate bodies into the lower crust (Glazner, 1994). Alternatively, if differentiation of basalt occurs at deep levels in the crust then the complementary dense mafic cumulates will be located in the lower crust (e.g. Debari & Coleman, 1989; Müntener *et al.*, 2001) where they may eventually delaminate into the mantle below (Kay & Kay, 1993; Jull & Keleman, 2001) thereby progressively driving the bulk crust towards andesite composition. The silica-rich residual melts generated by deep-seated basalt differentiation can be extracted and ascend, either to erupt immediately or to stall to form shallow magma chambers. If unerupted, such shallow chambers consolidate to form granite plutons, with mafic igneous rocks being a minor component or absent.

Recent numerical simulations of heat transfer (Annen & Sparks, 2002) and high-temperature experiments (Müntener *et al.*, 2001; Prouteau & Scaillet, 2003) suggest a model whereby silica-rich magmas can be generated by incomplete crystallization of hydrous basalt at upper mantle and/or lower crustal depths. These observations motivate our development of a model in which basalt emplacement into the lower crust leads to generation of intermediate and silicic melts (Fig. 1). Our model builds upon the concept of underplating (Raia & Spera, 1997), expands on models of differentiation of basalt at high pressure (Gill, 1981; Grove *et al.*, 2002) and incorporates aspects of AFC (DePaolo, 1981) and MASH (Hildreth & Moorbath, 1988). We develop a quantitative model in which evolved melts are generated from H_2O-rich parental basalts both by partial crystallization of the basalts themselves and by partial melting of surrounding crustal rocks through heat and H_2O transfer from the cooling basalts. A key feature of our model is that melt compositions are determined by the depth of emplacement of individual basalt intrusions and thermal equilibration with the local geotherm. We refer to the site of basalt injection and melt generation in the lower crust as a deep crustal hot zone. Previous models of underplating (e.g. Huppert & Sparks, 1988; Bergantz, 1989; Raia & Spera, 1997; Petford & Gallagher 2001; Jackson *et al.*, 2003) have concentrated almost exclusively on melt generated

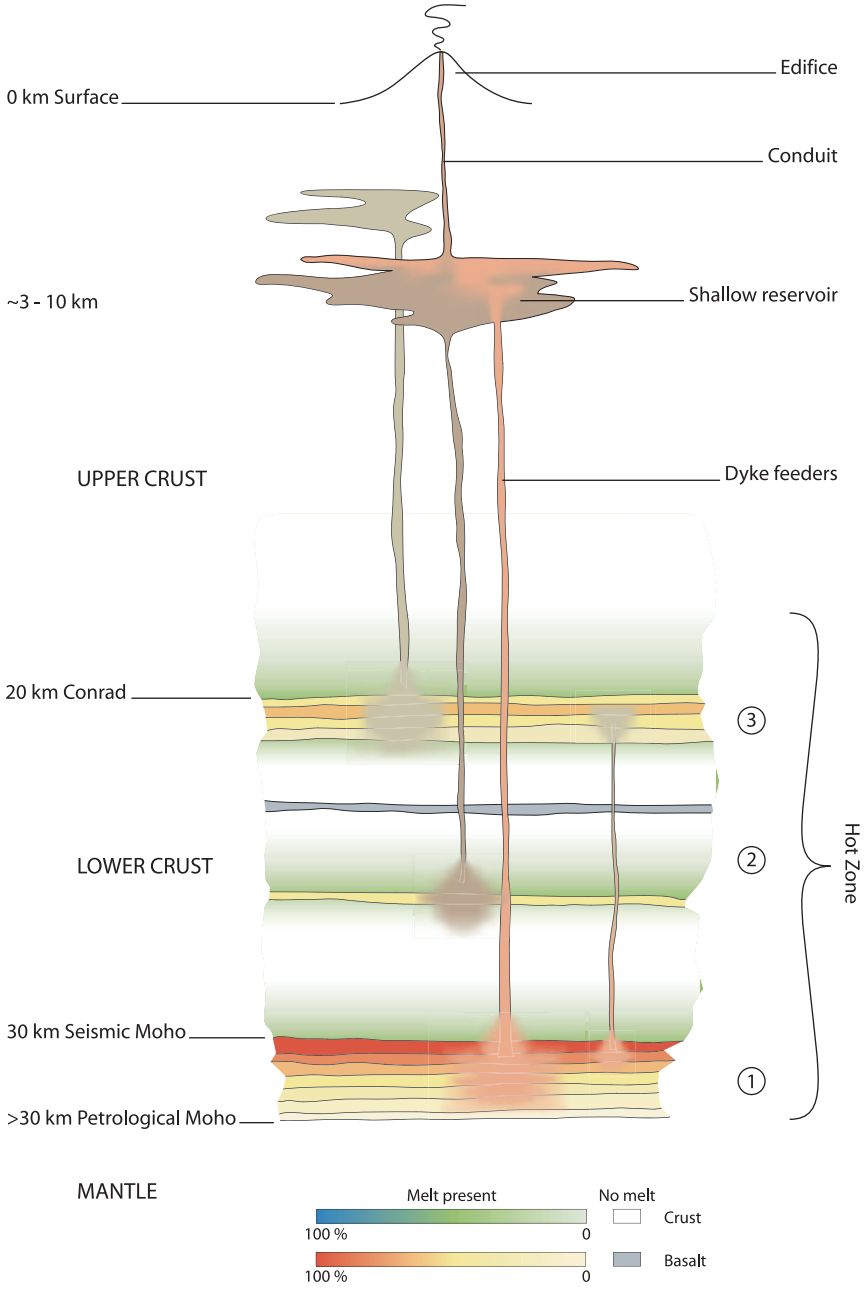

Fig. 1. Conceptual representation of a hot zone (not to scale). Sills of mantle-derived basaltic magma are injected at a variety of depths, including (1) the Moho, (2) the lower crust and (3) the Conrad Discontinuity between lower and upper crust. Sills injected at the Moho displace older sills into the mantle, creating a contrast between the petrological Moho (base of sill complex) and seismological Moho (top of sill complex). Sills crystallize from their injection temperature to that of the geotherm, resulting in a wide variety of residual melt fractions at any given time, from near 100% (newly injected sill near Moho) to 0% (old sill injected into lower crust). The fraction of crustal melt varies throughout the hot zone according to the age and proximity of the basalt sills. Melts ascend from the hot zone to shallow storage reservoirs, leaving behind dense refractory cumulates or restites. Residual and crustal melts from different portions of the hot zone may be mixed together prior to ascent or within the shallow reservoir.

by heating of the crust, with less attention paid to the residual melt generated by partial crystallization of the underplated basalt intrusions. Here we develop the concepts proposed by Annen & Sparks (2002) and consider the full range of possible mechanisms of melt generation in the hot zone, including residual melt from basalt crystallization and partial melting of surrounding crustal rocks (Fig. 1). We then consider the evolution of

these melts as they are extracted from their source rocks and ascend to shallow crustal levels, degassing and crystallizing en route. The model is developed primarily for application to the genesis of subduction zone volcanic and plutonic rocks, and we will refer collectively to this whole suite of intermediate and silicic rock types as 'andesite', except where a compositional or textural distinction is relevant. However, our model has general applicability to other tectonic settings, including continental rift zones where plume-related basaltic magmas are intruded into the base of the continental crust.

SOURCES AND MECHANISMS FOR INTERMEDIATE AND SILICIC MAGMA GENERATION

There are five currently popular models for the generation of andesites (*sensu lato*), as follows.

Model I. Partial melting of harzburgite in the mantle wedge, fluxed by H_2O-rich fluids or melts liberated from the subducting slab (e.g. Tatsumi, 1982; Hirose, 1997; Blatter & Carmichael, 2001; Carmichael, 2002, 2004; Parman & Grove, 2004).

Model II. Crystallization of mantle-derived basalt or basaltic andesite in shallow crustal magma chambers (e.g. Sisson & Grove, 1993; Grove *et al.*, 1997; Pichavant *et al.*, 2002*b*).

Model III. Crystallization of mantle-derived basalt or basaltic andesite in the deep arc crust at or close to the Moho (e.g. Müntener *et al.*, 2001; Annen & Sparks, 2002; Mortazavi & Sparks, 2003; Prouteau & Scaillet, 2003).

Model IV. Dehydration partial melting of meta-basalts (amphibolites) in the lower or middle crust by intrusions of hot, mantle-derived magma (e.g. Smith & Leeman, 1987; Petford & Atherton, 1996; Jackson *et al.*, 2003).

Model V. Mixing between silicic magmas and mantle-derived mafic magmas (e.g. Heiken and Eichelberger, 1980). In some cases the silicic component is generated by partial melting of crustal rocks (e.g. Druitt *et al.*, 1999).

In this paper we focus on Models III–V, which take place in the middle or lower crust. Models I and II are briefly considered first. Generation of andesite by mantle melting (Model I) has been demonstrated experimentally (Tatsumi, 1982; Hirose, 1997; Grove *et al.*, 2002, 2003; Parman & Grove, 2004) and calculated thermodynamically (Carmichael, 2002, 2004). The andesites produced in this way have elevated MgO contents and high mg-numbers, a requirement for equilibrium with the Mg-rich olivines of mantle harzburgite. Boninite series magmas are widely thought to originate by H_2O-fluxed melting of harzburgite (Falloon & Danyushevsky, 2000; Parman & Grove, 2004), whereas the generation of 'high-Mg andesites' may involve reactions between ascending slab-derived silicic melts and mantle peridotite (Yogodzinsky & Kelemen, 1998). However, high-Mg andesites and boninites are not the dominant rock types of volcanic arcs; typical arc andesites, with low mg-numbers, could not have been in direct equilibrium with mantle rocks.

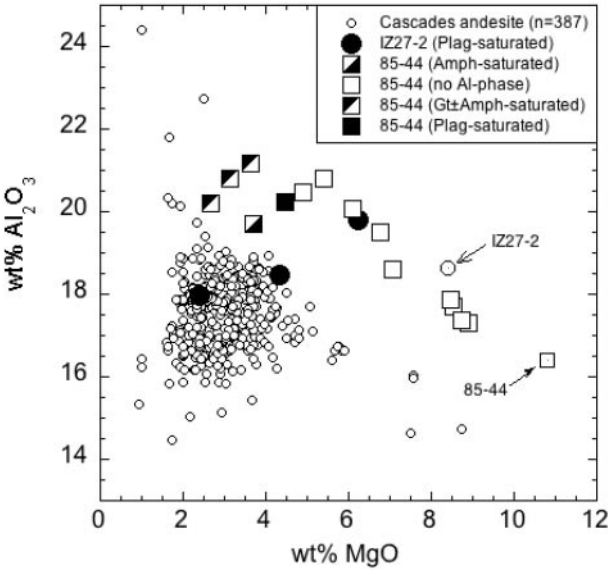

Fig. 2. Compositions of experimentally produced residual melts from crystallization of hydrous basalts in the lower crust. Squares denote melt compositions from experiments on a primitive Mount Shasta basaltic andesite, sample 85-44 (mg-number 0·71), from Müntener *et al.* (2001) and Grove *et al.* (2003), at 0·8–1·2 GPa, 1045–1230°C and with ≥2·5 wt % added H_2O; filled circles denote experimental melts from Kawamoto (1996) on a Higushi-Izu high alumina basalt, sample IZ27-2 (mg-number 0·60), at 1·0 GPa, 1000–1150°C with 1 wt % added H_2O. The compositions of the two different starting materials are indicated. Symbols that are filled or partially filled denote glasses in equilibrium with an aluminous phase, as shown in the legend. All of the IZ27-2 glasses are saturated in plagioclase. For reference the compositional field defined by 387 published analyses of Cascades andesites is shown. It should be noted that >96% of these andesites contain <19 wt % Al_2O_3.

Model II is widely favoured. Basalt and basaltic andesite lavas occur at many arc stratovolcanoes and occasionally contain xenoliths of cumulate origin (e.g. Arculus & Wills, 1980). Several experimental studies demonstrate that andesite can be generated by fractional crystallization of H_2O-saturated basalts and basaltic andesites at $pH_2O = P_{tot}$ of 200–400 MPa and temperatures of 950–1050°C (Sisson & Grove, 1993; Grove *et al.*, 1999, 2003; Pichavant *et al.*, 2002*b*) by crystallizing an assemblage of plagioclase ($An_{60–90}$) + clinopyroxene + amphibole + oxides ± orthopyroxene ± olivine. One constraint on the origin of andesites is that they typically contain <19% Al_2O_3 (Fig. 2), indicating that by the time residual melts have attained >57 wt % SiO_2 they have become saturated in an aluminous phase. In Model II

crystallization of plagioclase serves to limit Al_2O_3 enrichment in residual melts. The lack of abundant dense complementary mafic to ultramafic cumulate rocks in the shallow crust is problematic for Model II unless the associated mafic cumulates are removed by sinking (Glazner, 1994).

Model III involves fractional crystallization of similar parental magmas to Model II, but at higher pressure, thereby obviating the problem of the missing mid- or upper-crustal mafic cumulates. Mantle-derived magmas intruded into the deep crust cool and crystallize producing evolved residual melts. The principal difference between high- and low-pressure crystallization of hydrous basalt lies in the nature of the crystallizing assemblage. At higher pH_2O garnet (e.g. Wolf & Wyllie, 1994; Rapp, 1995) and aluminous amphibole (Grove *et al.*, 2003) are stabilized and can contribute to minimizing Al_2O_3 enrichment in residual melts. Conversely, plagioclase stability is reduced and liquidus plagioclase is anorthite-rich, a common finding in arc-related cumulate nodules (e.g. Arculus & Wills, 1980). In terms of melt chemistry, it is very hard to distinguish between residual melts produced by crystallization of *An*-rich plagioclase and pyroxenes from H_2O-undersaturated basalt at ~1·0 GPa (Kawamoto, 1996) and those produced from H_2O-saturated basalt at 0·2–0·4 GPa (e.g. Sisson & Grove, 1993; Pichavant *et al.*, 2002*b*). The appearance of garnet as the liquidus aluminous phase in andesite and dacite melts at pressures over ~1·1 GPa (Wolf & Wyllie, 1994; Rapp, 1995) imparts a distinctive trace element chemistry to residual melts (e.g. high Sr/Y), which provides a clear indication of high-pressure differentiation (e.g. Smith & Leeman, 1987; Feeley & Davidson, 1994; Feeley & Hacker, 1995).

In Models II and III, Al_2O_3 enrichment in derivative melts is further minimized if the primitive basalt itself has relatively low Al_2O_3. Circumstances for generation of such magmas are inferred in many arcs with a relatively depleted mantle wedge (Grove *et al.*, 2003; Parman & Grove, 2004). For example, primitive arc basalts with only 14–15% Al_2O_3 have been described for Klyuchevskoy volcano, Kamchatka (Ozerov, 2000).

When mafic magmas are intruded into the arc crust they transfer heat and volatiles (principally H_2O) into the surrounding crust, which can lead to partial melting of the wall-rocks. The deep crustal hot zone is, therefore, envisaged as a mixture of partially crystallized basalt, partially molten crustal rocks and H_2O liberated from the solidifying basalts (Fig. 1). Geophysical evidence is consistent with these concepts. In the Cascades, for example, the release of significant volumes of H_2O from deeply intruded basalts may account for the presence of a highly electrically conductive layer at 10–30 km depth (Stanley *et al.*, 1990), and in the central Andes a broad conductive zone (Brasse *et al.*, 2002) is associated with a low-velocity zone at depths of 20–40 km (Yuan *et al.*, 2000), interpreted as a laterally extensive region of partial melt, capped by a silicic magma body ~1 km thick (Chmielowski *et al.*, 1999). Below volcanoes in the Japan arc broadband seismometers have recorded low-frequency tremors and micro-earthquakes at 30–50 km depth (Obara, 2002; Katsumata & Kamaya, 2003). These can be explained by deformation associated with magma intrusions (S. Sachs, personal communication, 2003) and their low frequency is consistent with the presence of a fluid phase. Finally, beneath central North Island, New Zealand, a seismically highly reflective layer at 35 km depth, interpreted as a body of partially molten rock (Stratford & Stern, 2004), suggests that beneath some arcs the hot zone may be located in the uppermost mantle, rather than within the crust, which is only 16 km thick in this region.

The partially molten crust surrounding the basalt may be older intrusions of related mantle-derived hydrous basalt (or amphibolite) or unrelated metamorphic arc crust. This is Model IV. The volume and composition of the partial melt produced depends on the intrusion rate (heat flux) of the mantle-derived basalts, the prevailing geotherm and the extent to which the melting region is fluxed by H_2O liberated from the crystallizing basalt. Chemically hybrid melts can be formed if the residual melts from basalt crystallization are mixed with crustal partial melts during extraction, ascent and shallow intrusion; this is Model V.

Models III and IV both involve partially molten hydrous basaltic rocks in the lower crust produced, respectively, by crystallization and melting. Deep-seated crystallization of hydrous basaltic magmas differs from dehydration melting of the lower crust, as modelled by Raia & Spera (1997), Petford & Gallagher (2001) and Jackson *et al.* (2003), in one fundamental regard, the availability of H_2O. In dehydration melting the H_2O content of the source rock is strictly limited by the amount of H_2O that can be structurally bound in hydrous minerals such as amphibole and mica. For a mafic amphibolite with 40% amphibole, this amounts to ~0·8 wt % H_2O. Greater quantities of H_2O can be involved only if the heat source efficiently fluxes the source region with H_2O. Although this is likely, no extant models of crustal melting consider this process, largely because it is uncertain whether H_2O passing through a low-porosity source rock triggers melting or is simply carried away along fractures. By contrast, deep-seated crystallization of hydrous arc basalt magmas has no such upper limit on H_2O content. Studies of melt inclusions in primitive arc magmas, together with high-pressure experiments, indicate dissolved H_2O contents from almost zero to 10 wt % (e.g. Sisson & Layne, 1993; Carmichael, 2002; Pichavant *et al.*, 2002*a*; Grove

et al., 2003). The wide range of H_2O contents and bulk compositions of parental arc basalts ensures that crystallization of hydrous basalt can generate a wide diversity of residual melt compositions, as demonstrated experimentally by Sisson *et al.* (2005).

Dehydration melting (Model IV) requires a heat source. In arcs the widespread association of evolved igneous rocks with mantle-derived basalt strongly suggests that mafic magmas provide the heat source (Hildreth, 1981). However, herein lies a problem: models of heat transfer show that arc basalts emplaced into the base of the crust at temperatures of 1100–1240°C (see Ulmer, 2001; Pichavant *et al.*, 2002*a*) cannot provide enough heat to melt amphibolite lower crust extensively (Petford & Gallagher 2001; Annen & Sparks, 2002), because of the high dehydration melting temperature of amphiboles in mafic rocks (~950°C). More fertile upper crustal pelitic protoliths can be melted more efficiently, but large amounts of basalt are still needed as a heat source (Annen & Sparks, 2002). In addition, silicic rocks in arcs are typically calc-alkaline and metaluminous, which places limits on the amount of pelite that can be melted. The isotopic and geochemical signatures of evolved plutonic and volcanic arc rocks clearly indicate contribution from pelitic crust in some cases (DePaolo *et al.*, 1992), but significant amounts of basalt or meta-basalt (amphibolite) must be involved in their petrogenesis. The problem in arcs is how to generate large volumes of metaluminous, calc-alkaline evolved melts when the proposed amphibolite source is too refractory to undergo significant dehydration melting at plausible temperatures. This paradox can be solved if crystallization of H_2O-bearing mantle-derived basalt is the principal source of the evolved melts.

CRYSTALLIZATION OF ANDESITE IN THE SHALLOW CRUST

Once generated in the deep crust andesite and dacite residual melts can detach and ascend into the shallow crust. Subduction-related andesites and dacites are commonly porphyritic, with phenocrysts of plagioclase plus various proportions of hornblende, clinopyroxene, orthopyroxene, biotite and oxides; the exact ferromagnesian assemblage depends on magma composition, partial pressure of volatiles (especially pH_2O), oxygen fugacity (fO_2) and temperature (e.g. Rutherford *et al.*, 1985; Rutherford & Devine, 1988; Blatter & Carmichael, 1998, 2001; Moore & Carmichael, 1998; Scaillet & Evans, 1999; Pichavant *et al.*, 2002*b*; Izebekov *et al.*, 2004). Invariably the groundmass or matrix glass in porphyritic andesites and dacites is rhyolitic in composition. The phenocryst assemblages commonly have complex textures and zoning patterns, which indicate that magmatic evolution can involve processes such as: repeated mixing of different batches of magma (e.g. Heiken & Eichelberger, 1980; Clynne, 1999); entrainment of old crystals from previously consolidated magma batches (Davidson *et al.*, 1998, 2001, 2005; Heath *et al.*, 1998; Cooper & Reid, 2003; Reagan *et al.*, 2003; Dungan & Davidson, 2004) or from assimilation of crustal rocks (Ferrara *et al.*, 1989); convective stirring (Couch *et al.*, 2001); crystal growth induced by degassing (Blundy & Cashman, 2001). Whereas some of these phenocrysts grew from the magma in which they are found, others are entrained xenocrysts from earlier magma pulses or from chemically unrelated wall-rocks (e.g. Izebekov *et al.*, 2004; Davidson *et al.*, 2005). Detailed studies of volcano evolution (e.g. Bacon, 1983; Bacon & Druitt, 1988; Druitt & Bacon, 1989; Harford *et al.*, 2002) and constraints on timescales for crystallization (e.g. Zellmer *et al.*, 1999, 2003*a*, 2003*b*; Harford & Sparks, 2001) suggest that these various processes are the consequence of amalgamation of shallow magma bodies in the upper crust through many episodes of magma ascent from greater depths, sometimes accompanied by eruption. Field and geochronological evidence from calc-alkaline plutonic rocks ('granites', *sensu lato*) also supports their formation by amalgamation of many small intrusions, often of magmas with very similar bulk chemical composition but subtle textural differences (e.g. John & Blundy, 1993) or radiometric ages (e.g. Coleman *et al.*, 2004; Glazner *et al.*, 2004).

Our main concern here is to establish under what conditions the common phenocryst assemblages in andesites and granites are formed. Central to this issue are the H_2O contents and temperatures of andesite magmas. The importance of these two variables in interpreting the phenocryst assemblages and compositions of andesites has been investigated for over 30 years in a large number of experimental studies at pH_2O ($\leq P_{tot}$) of 0·1 to ≥400 MPa (Eggler, 1972; Green, 1972; Eggler & Burnham, 1973; Maksimov *et al.*, 1978; Sekine *et al.*, 1979; Rutherford *et al.*, 1985; Rutherford & Devine, 1988, 2003; Luhr, 1990; Foden & Green, 1992; Sekine & Aramaki, 1992; Sisson & Grove, 1993; Kawamoto, 1996; Grove *et al.*, 1997, 2003; Barclay *et al.*, 1998; Blatter & Carmichael, 1998, 2001; Moore & Carmichael, 1998; Cottrell *et al.*, 1999; Martel *et al.*, 1999; Sato *et al.*, 1999; Scaillet & Evans, 1999; Pichavant *et al.*, 2002*b*; Couch *et al.*, 2003; Prouteau & Scaillet, 2003; Barclay & Carmichael, 2004; Costa *et al.*, 2004; Izebekov *et al.*, 2004). Although many of these studies are focused on rocks from a specific volcano, some general conclusions can be drawn regarding subduction-related andesites and dacites, as follows.

(1) Eruption temperatures, as determined by geothermometry, are consistently less than low-pressure (<300 MPa) andesite liquidus temperatures even under

H_2O-saturated conditions. In many cases the difference is several tens of degrees and can be as much as 200°C (e.g. Blatter & Carmichael, 1998; Barclay & Carmichael, 2004).

(2) The liquidus phases at low pH_2O often include minerals (e.g. olivine, clinopyroxene) that are absent from the phenocryst assemblage in the natural rocks (e.g. Blatter & Carmichael, 1998, 2001; Scaillet & Evans, 1999; Costa *et al.*, 2004).

(3) Although amphibole is a common phenocryst it rarely occurs on the andesite liquidus at pH_2O <400 MPa even under oxidizing conditions; where it is stable, amphibole typically appears ≤100°C below the liquidus (e.g. Rutherford & Devine, 1988, 2003; Blatter & Carmichael, 1998, 2001; Moore & Carmichael, 1998; Martel *et al.*, 1999; Costa *et al.*, 2004; Izebekov *et al.*, 2004).

(4) Plagioclase is stabilized only at low pH_2O and is rarely a true liquidus phase at pH_2O >100–200 MPa, even though plagioclase is a ubiquitous phenocryst phase in most andesites (e.g. Eggler, 1972; Maksimov *et al.*, 1978; Sekine *et al.*, 1979; Sekine & Aramaki, 1992; Blatter & Carmichael, 1998, 2001; Moore & Carmichael, 1998; Martel *et al.*, 1999; Grove *et al.*, 2003).

(5) The anorthite (*An*) content of plagioclase increases with increasing pH_2O (at constant temperature) and increasing temperature (at constant pH_2O). For a given andesite, plagioclase phenocryst rims typically have considerably lower *An* contents (by up to 30 mol %) than the experimentally determined liquidus or near-liquidus plagioclase (e.g. Rutherford *et al.*, 1985; Scaillet & Evans, 1999; Rutherford & Devine, 2003; Costa *et al.*, 2004).

(6) The observed phenocryst assemblage, phase compositions and crystallinity typically are consistent with H_2O-saturated conditions at pressures of 100–300 MPa and at sub-liquidus temperatures consistent with those obtained from mineral thermometry on the natural rocks (e.g. Blatter & Carmichael, 1998; Moore & Carmichael, 1998; Martel *et al.*, 1999; Costa *et al.*, 2004).

The similarity of phase proportions and compositions in both experiments and natural andesites (Fig. 3) indicates that, to a first approximation, these magmas have undergone near-closed system crystallization from an initial fully molten state to a porphyritic magma under conditions of low-pressure H_2O-saturation. However, very few of the studied andesites contain their full complement of experimentally determined liquidus phases under these conditions, suggesting that either magma temperatures were never high enough to form a fully molten andesite liquid at low pressure or that the original liquidus phases were completely eliminated (or re-equilibrated) by reaction with the melt. The interpretation we favour is that andesite liquids, once formed and extracted from the deep crust, typically crystallize under polybaric conditions, at temperatures that do not significantly exceed their eruption temperature. Thus the initial fully molten state of an andesite is not a consequence of high temperature, but a consequence of high pH_2O. All of the above observations [(1)–(6)] are consistent with this interpretation, as are the observed zoning patterns and rim compositions of plagioclase phenocrysts (Fig. 3). For example, the phenocryst assemblage and proportions of the Colima andesite (Fig. 3a) can be reproduced closely at 950–960°C (consistent with mineral thermometry on the natural lava) and pH_2O from 70 to 150 MPa (Moore & Carmichael, 1998). The very calcic cores of some plagioclase phenocrysts ($An_{\leq 85}$) were ascribed by Moore & Carmichael (1998) to the onset of crystallization at even higher pH_2O but at essentially the same temperature. Using analyses of phenocryst-hosted melt inclusions, Blundy & Cashman (2005) advanced a similar argument for the silicic andesites of Mount St. Helens. They proposed that the observed phenocryst assemblage of the white pumice of 18 May 1980 crystallized in response to decompression from 233 to 140 MPa at a near-constant temperature of ~900°C, whereas the subsequent microlite-bearing dome lavas continued to crystallize down to pressures as low as 9 MPa with negligible cooling. Another example is the Soufrière Hills andesite, Montserrat, where $An_{50–60}$ plagioclase inclusions in the cores of amphibole phenocrysts (Higgins & Roberge, 2003), combined with experimental data (Couch *et al.*, 2003; Rutherford & Devine, 2003), indicate protracted polybaric crystallization at temperatures sufficiently low to stabilize amphibole (840–880°C; Murphy *et al.*, 2000; Devine *et al.*, 2003; Rutherford & Devine, 2003). Major element chemistry of whole-rocks, phenocrysts and groundmass glass (Murphy *et al.*, 2000; Harford *et al.*, 2002) is consistent with crystallization of predominantly amphibole and plagioclase from a liquid whose initial andesite composition evolved to rhyolite as crystallization proceeded.

All of the above examples suggest that decompression crystallization can play a major role in determining the crystallization sequence, assemblage and proportions. That is not to say that cooling is not important in some circumstances, nor that reheating caused by magma mixing does not occur: there is compelling evidence for both processes in many andesite magmas.

An attractive attribute of polybaric, decompression-driven crystallization is that it can be very rapid in comparison with the slow rates of crystallization expected for cooling-driven crystallization caused by heat loss from shallow magma chambers. For example, consider the case of H_2O-saturated Colima andesite. To generate the observed phenocryst proportions by isobaric cooling alone would require a temperature drop of some 125°C at pH_2O = 70 MPa (Moore & Carmichael, 1998). To attain the same crystallinity by isothermal decompression

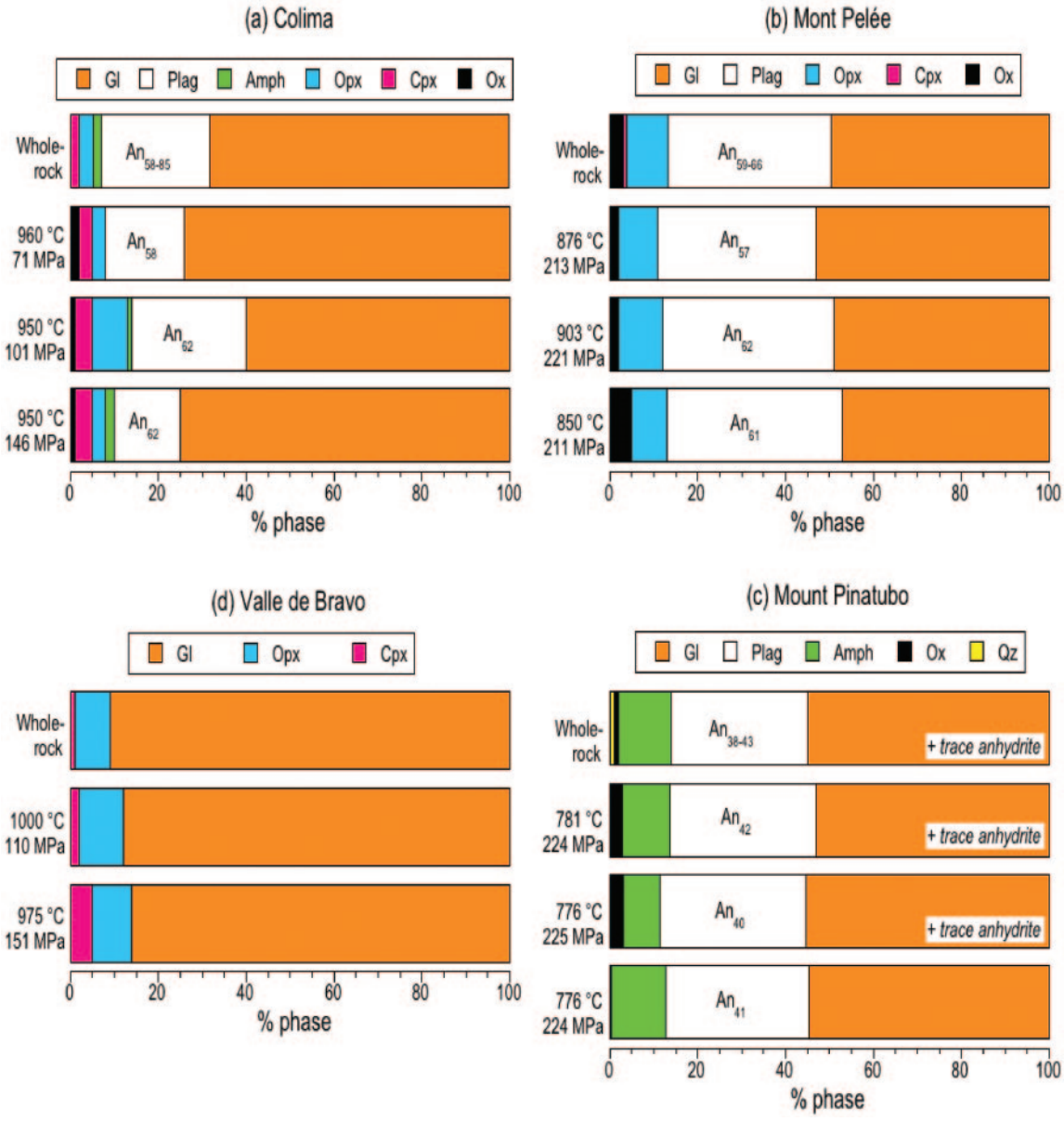

Fig. 3. Comparison of experimental and natural whole-rock phase proportions (weight percent) for selected andesite compositions. (a) Volcán Colima, Mexico (Moore & Carmichael, 1998); (b) Mont Pelée, Martinique (Martel *et al.*, 1999); (c) Mount Pinatubo, Philippines (Scaillet & Evans, 1999; B. Scaillet, personal communication, 2004); (d) Valle de Bravo, Mexico (Blatter & Carmichael, 2001). All experiments are H_2O-saturated at the pressure and temperature shown. Only experiments in which the temperature is close to that inferred from mineral thermometry of the whole-rock are shown. Also shown is the molar anorthite (*An*) content of plagioclase. gl, glass; plag, plagioclase; amph, amphibole; opx, orthopyroxene; cpx, clinopyroxene; ox, oxide.

(at 960°C) would require a pressure drop of 60 MPa, equivalent to an ascent of ~2 km. A pressure drop can be achieved much more rapidly than a temperature drop, as follows.

Cooling of shallow magma chambers is controlled by conduction through the wall-rocks and convection within the magma body and the superjacent hydrothermal system (Carrigan, 1988). The cooling timescale is controlled by the magma chamber size and the vigour of hydrothermal convection. The world's most active geothermal systems associated with large silicic magma chambers have convective thermal fluxes of several W/m^2 (Carrigan, 1988). Assuming that the magma chamber convects internally, then the heat loss from the chamber

can be converted into the time required to cool the chamber to a given temperature by a heat balance calculation. For example, for a cylindrical chamber with 1 km radius and 1 km depth (a volume of $\sim 3\,km^3$), the time to cool the magma internally by $\sim 100°C$ is calculated at 8400 years for a heat flow of $2{\cdot}2\,W/m^2$ and a heat loss of 220 kJ/kg assuming 20% crystallization, a latent heat of 419 kJ/kg and heat capacity of 1361 kJ/kg per K. Larger chambers or lower hydrothermal heat fluxes would increase crystallization times significantly.

In contrast, magma ascent into the shallow crust is envisaged to occur in dykes (Petford *et al.*, 1993) at speeds of cm/s to dm/s. The time taken for an H_2O-saturated andesite melt to ascend 2 km would be a matter of hours (Lister & Kerr, 1991; Petford *et al.*, 1993), thereby generating a significant undercooling caused by gas exsolution, leading to rapid nucleation and growth of crystals. Rapid crystallization of phenocrysts in arc magmas is consistent with U-series data (Reagan *et al.*, 2005) and diffusion dating studies of phenocrysts (Zellmer *et al.*, 1999, 2003*b*; Costa *et al.*, 2004), which suggest crystallization on timescales that are far more rapid than would be expected for crystallization driven by cooling alone. Rapid crystallization also provides an effective means of generating the near-closed system crystallization inferred from experimental studies, because the timescales are too short to permit significant crystal–melt segregation, for example by crystal settling. The physical consequences of decompression crystallization are discussed further in a later section.

Whatever the cause of crystallization, the experimental data present a compelling argument that the chemical composition of andesites is determined at depth, prior to magma emplacement in the shallow crust. Of course, this concept does not exclude subsequent processing of andesite magmas in shallow chambers, including magma mixing and more advanced fractional crystallization. For example, at Santorini, Greece, dacites and rhyolites can be demonstrably related to andesite by low-pressure fractional crystallization of orthopyroxene–clinopyroxene–plagioclase–oxide assemblages (Nicholls, 1971; Druitt *et al.*, 1999), whereas at Crater Lake, USA, rhyolite magma accumulated prior to the climactic eruption of Mount Mazama by repeated injection of andesite magmas into a shallow chamber, and extraction of residual rhyolitic melts by filter pressing (Sisson & Bacon, 1999). Partially solidified andesitic bodies, or 'proto-plutons', with >50% crystals can also be remobilized by subsequent pulses of hot magma from below, as envisaged at Soufrière Hills (Couch *et al.*, 2003) and Fish Canyon Tuff, USA (Bachmann & Dungan, 2002). There are also examples of zoned plutons, such as Boggy Plain, Australia (Wyborn *et al.*, 2001) where *in situ* fractionation from andesite to more evolved magmas has occurred. Additionally, such magma bodies are likely to develop incrementally over long periods of time so that mixing occurs between rising batches of andesite from depth (Fig. 1). The key concept is that the starting point for shallow chamber processes (e.g. further fractionation, wall-rock assimilation, magma mixing, magma recharge, repeated remobilization, etc.) is andesite, itself generated at greater depths.

EVIDENCE FOR HIGH H_2O CONTENTS IN ARC MAGMAS

Observations (Anderson, 1979; Murphy *et al.*, 2000; Cervantes & Wallace, 2003) and experimental studies (e.g. Sisson & Grove, 1993; Pichavant *et al.*, 2002*a*; Barclay & Carmichael, 2004) indicate that many arc basalts have H_2O contents in the range 2–6 wt %. Evolved residual melt obtained by crystallization of such basalts will be even more H_2O-rich provided that the pressure is high enough for H_2O to remain in solution. For example, 60% crystallization of basalts with 2–6 wt % H_2O can generate intermediate to silicic melts with H_2O contents of 5–15 wt %. (The figure is only slightly less if amphibole or mica are crystallizing phases.) Estimates of H_2O contents in calc-alkaline intermediate and silicic magmas commonly yield values of 4–6 wt % (Anderson, 1979; Green, 1982; Barclay *et al.*, 1998; Devine *et al.*, 1998; Carmichael, 2002, 2004; Blundy & Cashman, 2005), although andesite melt inclusions with up to 10% H_2O have been reported (Anderson, 1979; Grove *et al.*, 2003). These estimates are principally based on comparison of natural phenocryst assemblages with experimental products and/or melt inclusion studies. Both approaches provide good estimates of pre-eruption H_2O contents during the later stages of magma crystallization, but do not necessarily constrain H_2O contents at earlier stages of magma genesis. For example, Carmichael (2002, 2004) inferred from experimental phase equilibria and thermodynamic calculations that andesites erupted in west–central Mexico crystallized by decompression from a melt with an original H_2O content of at least 6 wt %, and possibly as much as 16 wt %, almost all of which was lost during magma ascent and eruption.

Additional experimental evidence for elevated H_2O contents in arc magmas comes from the presence of aluminous amphibole phenocrysts in andesites. At Mount Shasta, USA, Grove *et al.* (2003) showed that pargasitic amphibole (9–12 wt % Al_2O_3) overgrowth rims on magnesian olivine and pyroxenes are consistent with amphiboles produced experimentally from H_2O-saturated magnesian basalt at 800 MPa. At this pressure the dissolved H_2O content of the melts is estimated at ~ 14 wt %. At Mount Pinatubo, Philippines,

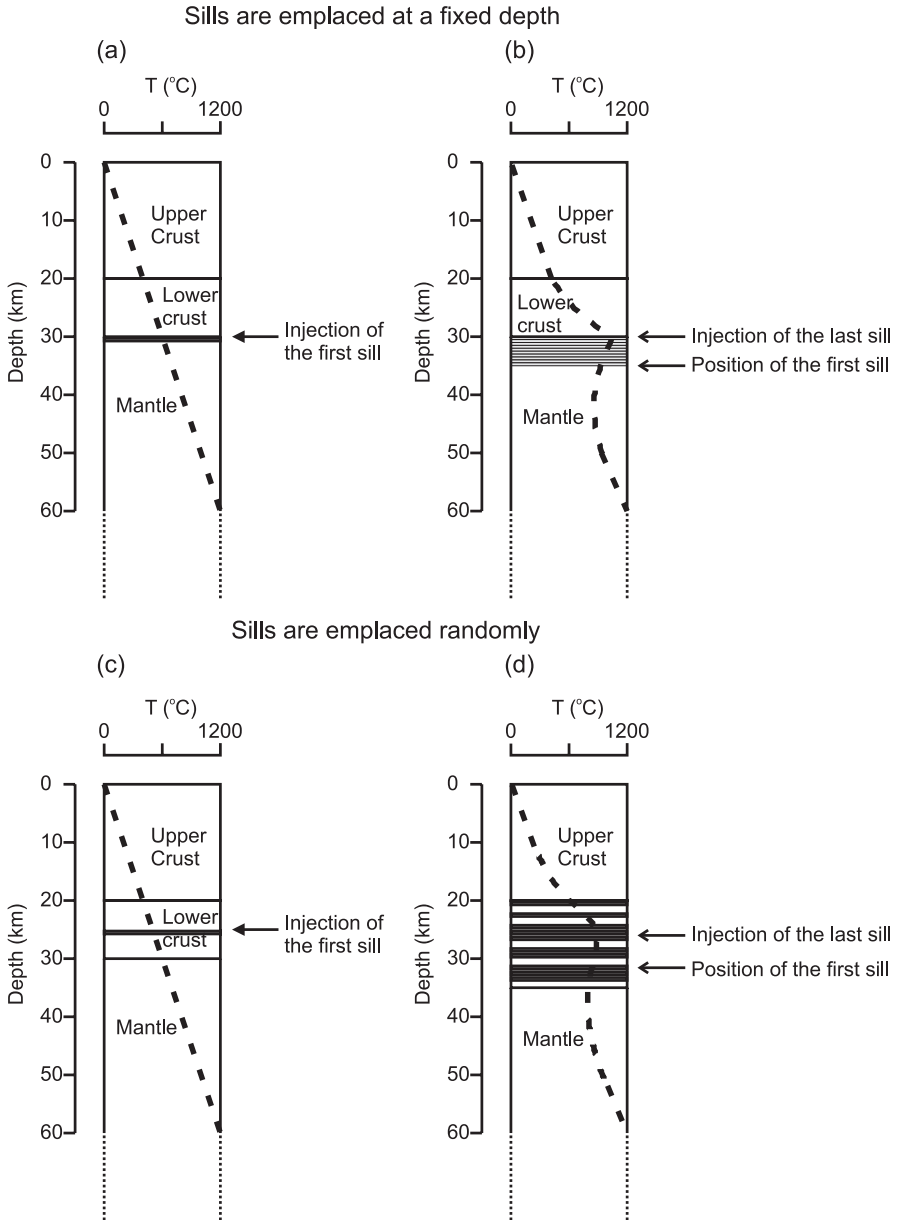

Fig. 4. Schematic representation of the evolution of the modelled hot zone. Basalt sills are emplaced at a fixed depth (a, b) or at random throughout the lower crust (c, d). The system is shown at the onset of intrusion (a, c) and after the emplacement of a series of sills (b, d). Each new sill volume is accommodated by downward displacement of the crust, previous sills and mantle below the injection level. Temperature is represented by the dashed line. The initial temperature is determined by a geothermal gradient of 20°C/km. The temperature of individual sills evolves with time and with their evolving position along the geotherm. The temperatures at the Earth's surface and at 60 km depth are fixed.

Prouteau & Scaillet (2003) observed aluminous cores (>11 wt % Al_2O_3) to some amphibole phenocrysts in the 1991 dacite. Amphiboles of similar composition were produced in H_2O-undersaturated experiments on the same dacite at pressures of 960 MPa, under which conditions melt H_2O contents exceed 10 wt %. Prouteau & Scaillet (2003) attributed the aluminous amphibole cores to generation of the 1991 dacite by crystallization of a basaltic parent melt near the base of the arc crust. The lower Al_2O_3 amphibole rims correspond to later crystallization at ~200 MPa in the sub-volcanic magma chamber.

In summary, the available petrological and experimental data are consistent with the derivation of

Table 1: Parameters used in the model

ρ	Density (kg/m^3)	Injected basalt	2830
		Lower crust	3050
		Upper crust	2650
C_p	Specific heat capacity (J/kg)	Injected basalt	1480
		Lower crust	1390
		Upper crust	1370
L	Specific latent heat (J/kg per K)	Injected basalt	$4{\cdot}0 \times 10^5$
		Lower crust	$3{\cdot}5 \times 10^5$
		Upper crust	$2{\cdot}7 \times 10^5$
k_0	Thermal conductivity at surface	Injected basalt	2·6
	temperature and pressure	Lower crust	2·6
	(J/s per m per K)	Upper crust	3·0
k	Thermal conductivity	$k = k_0(1 + 1{\cdot}5 \times 10^{-3}z)/$	
	(J/s per m per K)	$(1 + 1{\cdot}0 \times 10^{-4}T)$	

Sources: ρ, Holbrook *et al*. (1992) and Kay *et al*. (1992); C_p and L, Bohrson & Spera (2001); k_0 and k, Chapman & Furlong (1992). In the expression for thermal conductivity, z is the depth in kilometres, and T is the temperature in Kelvin.

H_2O-rich andesites by crystallization of hydrous, mantle wedge-derived basalt in a lower crustal hot zone.

MODELLING DEEP CRUSTAL HOT ZONES I—METHODS

We address the thermal development of a crustal hot zone with specific attention paid to all potential sites of melt generation, including partially crystallized basalt and partially melted crust. In our model a hot zone develops by injection of numerous discrete basaltic sills at the Moho or within the crust (Fig. 4). The thermal evolution of the hot zone, as a result of heat transfer between successive basaltic intrusions and country rock, is computed using the heat balance equation

$$\rho C_p \frac{\partial T}{\partial t} + \frac{\partial X}{\partial t}\rho L = k\frac{\partial^2 T}{\partial x^2} \qquad (1)$$

where ρ is density, C_p is specific heat capacity, T is temperature, t is time, X is melt fraction, L is latent heat of fusion, k is thermal conductivity and x is (vertical) distance. The system is discretized into a one-dimensional array of cells, and equation (1) is solved by forward finite difference and iterative methods. The code was written with Delphi 4© in Object Pascal language. The resolution of the finite difference cells is 25 m.

Between the liquidus and solidus the finite difference equivalent to equation (1) is solved by iterative approximation:

$$\rho c\frac{T_i^{p+1} - T_i^P}{\Delta t} + L\frac{X_i^{p+1} - X_i^p}{\Delta t} = k\frac{T_{i-1}^p - T_i^p}{\Delta x^2} + k\frac{T_{i+1}^p - T_i^P}{\Delta x^2} \qquad (2)$$

where Δt is the time step between the time p and the time $p + 1$. Cells $i - 1$ and $i + 1$ are below and above cell i, respectively. Δt is limited by the cell dimension, Δx, and rock diffusivity to <8·5 years. Above the liquidus or below the solidus, the latent heat is zero and the temperature of cell i at time $p + 1$ is

$$T_i^{p+1} = \frac{\Delta t}{\rho c}\left(k\frac{T_{i-1}^p - T_i^p}{\Delta x^2} + k\frac{T_{i+1}^p - T_i^P}{\Delta x^2}\right) + T_i^P \qquad (3)$$

The values of the parameters used in the model are given in Table 1. For sills with a horizontal dimension of 20 km or more, the neglected lateral heat loss at the boundary of the system does not significantly affect the outcome for timescales of <4 Myr (Annen & Sparks, 2002). The basalt emplacement rate, the fertility of the crust, the temperature of the injected basalt, and the sill injection level all control the thermal evolution of the system, and the amount and composition of the melt generated (Annen & Sparks, 2002). The model is entirely conductive and static. The issue of melt segregation process is discussed below, but it is instructive to consider the static case first.

Temperature and melt fraction

Application of equation (2) requires knowledge of the variation of melt fraction X with temperature T. The liquidus temperature (T_L; $X = 1$) of a basalt varies with dissolved H_2O and MgO contents (Ulmer, 2001; Wood, 2004). The relationship between X and T was parameterized using experimental data. There is no single set of experiments on a primitive basalt with fixed H_2O content against which to calibrate X–T relationships from solidus to liquidus. Instead we have spliced together two datasets, one at low temperature and one at high temperature, for two different basalt compositions obtained at slightly different pressures (Fig. 5). For high temperatures (X >0·5) we have used the 1·2 GPa experimental data of Müntener *et al.* (2001) for a Cascades basaltic andesite (sample 85-44; 10·8 wt % MgO, mg-number 0·71) with initial H_2O contents of 5, 3·8 and 2·5 wt % (Fig. 5a), run at fO_2 close to QFM (the quartz–fayalite–magnetite buffer). For lower temperatures (X <0·4) we used the 0·7 GPa experiments of Sisson *et al.* (2005) on Cascades basalt (87S35A; 6·5 wt % MgO, mg-number 0·54) with 2·3 wt % H_2O (Fig. 5b). To match the fO_2 of the two datasets we have only used those experiments of Sisson *et al.* (2005) that are within 0·5 log units of QFM.

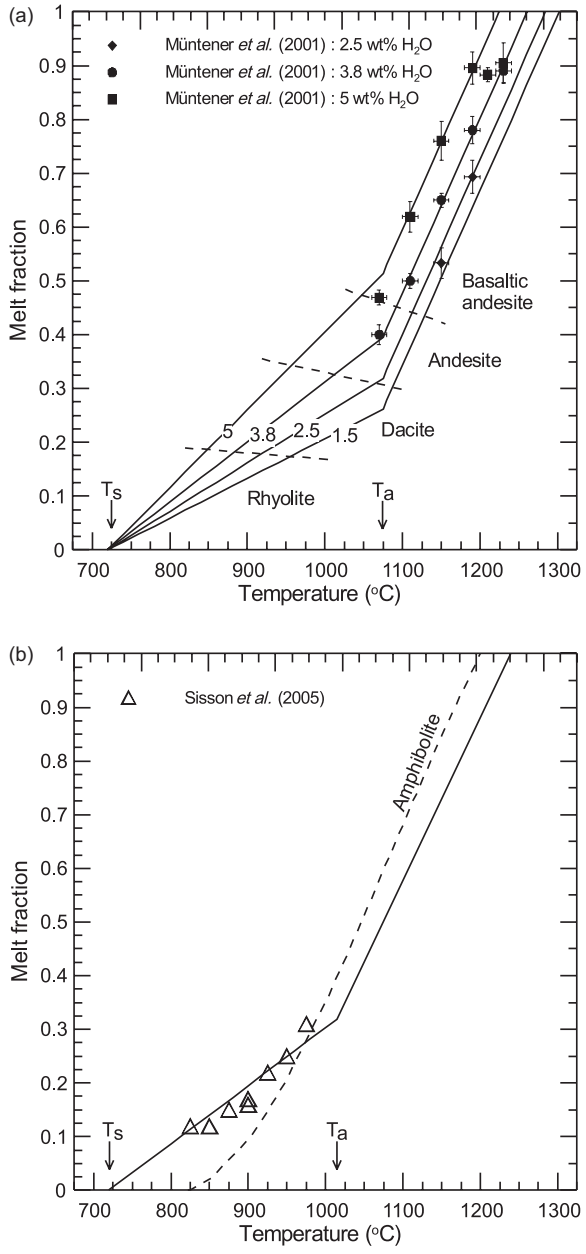

Fig. 5. Modelled melt fraction (X) vs temperature (T) curves for basalts. (a) At 1·2 GPa with, from left to right, initial H_2O contents of 5, 3·8, 2·5 and 1·5%. Symbols show experimental data from Müntener *et al.* (2001). The liquidus temperature (T_L) of basalt with 3·8 wt % initial H_2O is estimated by extrapolation. T_L for basalts with 1·5, 2·5 and 5 wt % initial H_2O is calculated with equation (5). The curves have a slope of $0{\cdot}325^{\circ}C^{-1}$ between T_L and T_a. They kink at T_a to fall linearly to T_s, the H_2O-saturated basalt solidus. (b) At 1 GPa, the modelled basalt curve with 2·5 wt % initial H_2O shows a good fit to the experimental data points of Sisson *et al.* (2005). The dashed curve is the X–T variation for amphibolite lower crust (after Petford & Gallagher, 2001). At low temperature the basalt produces more melt than the amphibolite because H_2O concentrates in the residual melt. At higher temperatures the higher fertility of the amphibolite is attributed to its slightly more differentiated composition (see Petford & Gallagher, 2001). Dashed lines in (a) divide fields in which the residual melt composition is, broadly speaking, basaltic andesite, andesite and dacite.

For the modelled basalt we assumed linear X–T relationships between T_L and the onset of amphibole crystallization, T_a, and between T_a and the solidus, T_s:

$$X = 1 \quad T > T_L \tag{4a}$$

$$X = 3{\cdot}25 \times 10^{-3}(T - T_L) + 1 \quad T_L \leq T \leq T_a \tag{4b}$$

$$X = \frac{X_a}{T_a - T_s}(T - T_s) \quad T_a \leq T \leq T_s \tag{4c}$$

$$X = 0 \quad T < T_s. \tag{4d}$$

T_L was extrapolated from the 3·8 wt % H_2O experiment of Müntener *et al.* (2001) to 1261°C (Fig. 5a). Following Wood (2004) T_L varies with H_2O according to the relationship

$$\Delta T_L = 80\ (\text{wt \% } H_2O)^{0{\cdot}4} \tag{5}$$

where ΔT_L is the liquidus depression relative to an anhydrous basalt of the same composition. T_L was calculated with equation (5) to be 1225, 1285 and 1302°C for total H_2O contents of 5, 2·5 and 1·5 wt %, respectively (Fig. 5a) in good agreement with the variation in T_L of the experiments of Müntener *et al.* (2001). The solidus temperature (T_s; $X = 0$) of basalt also depends on H_2O content. However, for any basalt that contains more H_2O than can be accommodated in subsolidus hydrous phases, principally amphibole for arc basalts, the appropriate solidus is that for H_2O saturation. Amphibole contains ~2 wt % H_2O and 40 wt % amphibole is an approximate upper limit for a basaltic composition amphibolite. Thus, for basalts with $\geq$0·8 wt % we have adopted the experimentally determined H_2O-saturated solidus of 720°C (Liu *et al.*, 1996).

The change of slope in the linear function at temperatures below the appearance of amphibole T_a [Fig. 5b; equation (4c)] is consistent with experimental data (e.g. Foden & Green, 1992; Kawamoto, 1999; Sisson *et al.*, 2005). In equation (4c), X_a is the melt fraction at T_a, calculated using equation (4b). We chose $T_a = 1075$°C based on the data of Müntener *et al.* (2001) data—the 1 GPa data of Foden & Green (1992) on a slightly more evolved arc basalt indicate a similar T_a of 1040°C.

The values of T_L and T_a are for a pressure of 1·2 GPa and are modified by 90 and 120°C/GPa, respectively (Foden & Green, 1992). We have not included here the effect of fO_2 on melt fractions and compositions, although we recognize that fO_2 can play a key role in controlling the stability of an oxide phase and the consequent SiO_2 enrichment at a given X (Osborn, 1957; Sisson *et al.*, 2005). Of course, at other subduction zones,

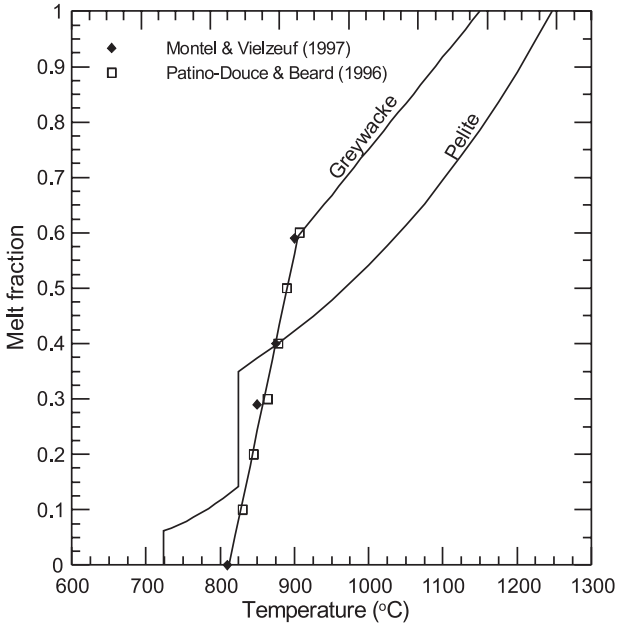

Fig. 6. Modelled melt fraction (X)–T curves for greywacke and pelite under upper crustal conditions. The greywacke curve is based on experimental data of Patiño-Douce & Beard (1996) and Montel & Vielzeuf (1997). The pelite curve is based on the model of Clemens & Vielzeuf (1987).

with different primary magma compositions, a different X–T parameterization may be more useful. However, at present there are insufficient experimental data available to make this worth while.

As X decreases so the SiO_2 content of the residual melts increases and MgO content decreases. An accurate parameterization of SiO_2 content would require additional experimental data as well as consideration of fO_2 and is beyond the scope of this paper. None the less we are able to sketch indicative contours of melt composition onto Fig. 5a as an approximate guide to how melt composition varies during basalt crystallization. Andesitic residual melts are generated at $0{\cdot}35 < X < 0{\cdot}50$, consistent with the experimental results of Kawamoto (1996) and Müntener *et al.* (2001), whereas the lower temperature experiments of Sisson *et al.* (2005) indicate that dacites and rhyolites are generated at $0{\cdot}20 < X < 0{\cdot}35$ and $X < 0{\cdot}20$, respectively.

For the upper crust lithology we have chosen two model compositions: a greywacke with 1·0 wt % structurally bound H_2O; and a fertile pelite with 1·2 wt % structurally bound H_2O (Fig. 6). The T–X relationships of the pelite are those adopted by Annen & Sparks (2002), based on the models of Clemens & Vielzeuf (1987). For the greywacke, we used a linear regression of experimental data from Patiño Douce & Beard (1996) and Montel & Vielzeuf (1997) below 900°C, and a linear function between 900°C and T_L, which has been taken as 1150°C (Fig. 6):

$$X = 1 \quad T > T_L \tag{6a}$$

$$X = 6{\cdot}36 \times 10^{-3} T - 5{\cdot}17 \quad T_L \leq T \leq 900^\circ\text{C} \tag{6b}$$

$$X = 1{\cdot}75 \times 10^{-3} T - 1{\cdot}017 \quad 900^\circ\text{C} \leq T \leq T_s \tag{6c}$$

$$X = 0 \quad T < T_s. \tag{6d}$$

The solidus temperature, T_s, is taken to be 812°C.

The model lower crust is an amphibolite for which we have adopted the experimentally constrained T–X relationship of Petford & Gallagher (2001). It should be noted that their model amphibolite has a more fertile bulk composition than the amphibolite modelled by Annen & Sparks (2002). Consequently, at a given temperature the amphibolite generates more melt than the hydrous mantle basalt, except close to the solidus where basalt melt fractions are higher (Fig. 5b). Melt generated by dehydration melting of pelite or greywacke is peraluminous in composition (Montel & Vielzeuf, 1997) and differs significantly from that generated by basalt crystallization or by amphibolite dehydration melting.

Basalt emplacement rate

We use an emplacement rate of 5 mm/year, corresponding to an addition rate of one 50 m basalt sill every 10^4 years. This value is representative of typical estimates of magma productivity in arcs (Crisp, 1984). We also tested intrusion rates of one 50 m basalt sill every 5×10^3 and every 25×10^3 years, corresponding to average intrusion rate of 10 and 2 mm/year, respectively. High intrusion rates result in fast rates of melt accumulation and high melt fractions, whereas low intrusion rates reduce or inhibit melt production. For a given emplacement rate, if the sill thickness is small compared with the total thickness of intruded basalt, the exact dimensions of sills only modify the details of the temperature and melt fraction on short timescales. As long as the repose period between sill intrusions (10^4 years) is much shorter than the total duration of basalt emplacement (10^6 years), the long-term evolution of the system is controlled by the average emplacement rate and is not affected by the details of sill thickness and injection frequency (Annen & Sparks, 2002). An intrusion rate of 5 mm/year is equivalent to 5 km of new crust per million years. Over several million years crustal thicknesses of tens of kilometres could be generated. However, our model does not consider the counteracting thinning processes such as spreading of hot thickened crust and delamination of dense lower crust.

Boundary and initial conditions

The boundary conditions are constant temperatures at the surface ($T = 0°C$) and at 60 km depth ($T = 1200°C$). The initial temperature variation with depth is determined by the geothermal gradient. Here we chose an initially linear geothermal gradient of 20°C/km. The upper crust, which is greywacke or pelite, is taken to be that part of the crust initially situated above 20 km depth; the amphibolite lower crust is initially situated between the Conrad Discontinuity at 20 km and the Moho at 30 km (Fig. 4). We have investigated intruding basalt magmas with 1·5 and 2·5 wt % H_2O.

Emplacement depth

Because the temperature through the hot zone varies with depth according to the geotherm, the basalt emplacement depth controls the temperature of equilibration of the intrusions and the consequent melt generation. We present results for two fixed emplacement levels, 30 km and 20 km (Fig. 4a and b), which model the Moho and Conrad discontinuities, respectively. We also tested a model where basalt sills are randomly emplaced in the lower crust (Fig. 4c and d). In all models, the thickness of each intruded sill is accommodated by downward displacement of the sequence below the sill resulting in a thickening of the crust and a downward displacement of the Moho. This type of accommodation is an approximation of isostatic equilibration.

MODELLING DEEP CRUSTAL HOT ZONES II—RESULTS

Sills are emplaced at the basalt liquidus temperature (T_L) appropriate for the chosen H_2O content. Each sill transfers its heat to the country rocks and equilibrates with the surrounding temperature, which depends on emplacement depth and the geotherm. With successive intrusions the temperature of the system progressively increases, the hot zone develops and the geotherm slowly evolves. Eventually new sills equilibrate above their solidus temperature and start to retain residual melt. Figures 7 and 8 show the evolution of temperature and melt fraction over time for a selection of 50 m sills emplaced every 10 kyr (Fig. 7) and every 25 kyr (Fig. 8) at 30 km depth (Figs 7a and 8a) and at 20 km depth (Figs 7b and 8b). Figures 7 and 8 depict the first sill (emplaced at time 0), the 50th sill (emplaced at time 500 kyr), the 100th sill (emplaced at time 1 Myr), and so on. The temperature and melt fraction of each sill evolve with its position on the geotherm, which changes shape with time as heat is supplied by successive sills (Fig. 4b and d).

When the solidus of the surrounding crust is reached it begins to undergo partial melting. Thus, melt in the hot zone ultimately comes from two distinct sources: from crystallization of basalt, which we refer to as *residual melt*; and from partial melting of crust, which we refer to as *crustal melt*. The crustal melt may derive from upper crust (greywacke or pelite) or lower crust (amphibolite). The relative contribution from each source depends on the thermal profile of the hot zone and the depth of basalt sill injection. In some cases the earliest intruded basalt sills will cool below their solidus, only to be heated above their solidus by subsequent basalt sills (Figs 7 and 8). In this case previously solidified basalt sills can be remelted. In detail these remelts may differ in composition from residual melts because of loss of volatiles on complete solidification. We have not, however, taken this subtle effect into account because a further parameterization is required (dehydration melting of hydrous mantle basalt), which is not well constrained by experiments. In practice, relatively little melt in the hot zone derives from remelting, and in the interests of simplicity we group all remelts with residual melts.

Incubation times

The incubation time is defined as the time between the emplacement of the first sill, which typically cools below its solidus, and the generation of the first silicic melt, whether as residual melt or crustal melt. The incubation time for residual and crustal melt strongly depends on basalt emplacement rate and emplacement depth (Fig. 9a). For a fixed emplacement depth at 30 km, the incubation time for residual melt generation varies from 260 kyr for an emplacement rate of 2 mm/year to 20 kyr for an emplacement rate of 10 mm/year (Fig. 9a). At shallow level the ambient temperature is lower and the incubation time for a given emplacement rate is significantly longer (Fig. 9a).

In the case of sills randomly emplaced in the lower crust between the Conrad and Moho discontinuities the heat advected by the basalts is distributed over the entire thickness of the lower crust, rather than being focused at one depth. Consequently, the incubation time is longer than in the case of fixed emplacement at 30 km or 20 km, except for a low emplacement rate of 2 mm/year (Fig. 9a). The incubation time for crustal melts depends on the depth of sill injection (Fig. 9b), but is typically greater than the corresponding incubation time for residual melt generation. One exception is for basalt emplaced in direct contact with fertile pelitic upper crust.

Hot zone efficiency and melt productivity

Figures 10 and 11 illustrate the efficiency of the system in generating melt for different emplacement levels and emplacement rates. Figure 10 shows the productivity of accumulated melt, i.e. the total thickness of residual or crustal melt generated for each 1 m of basalt injected in

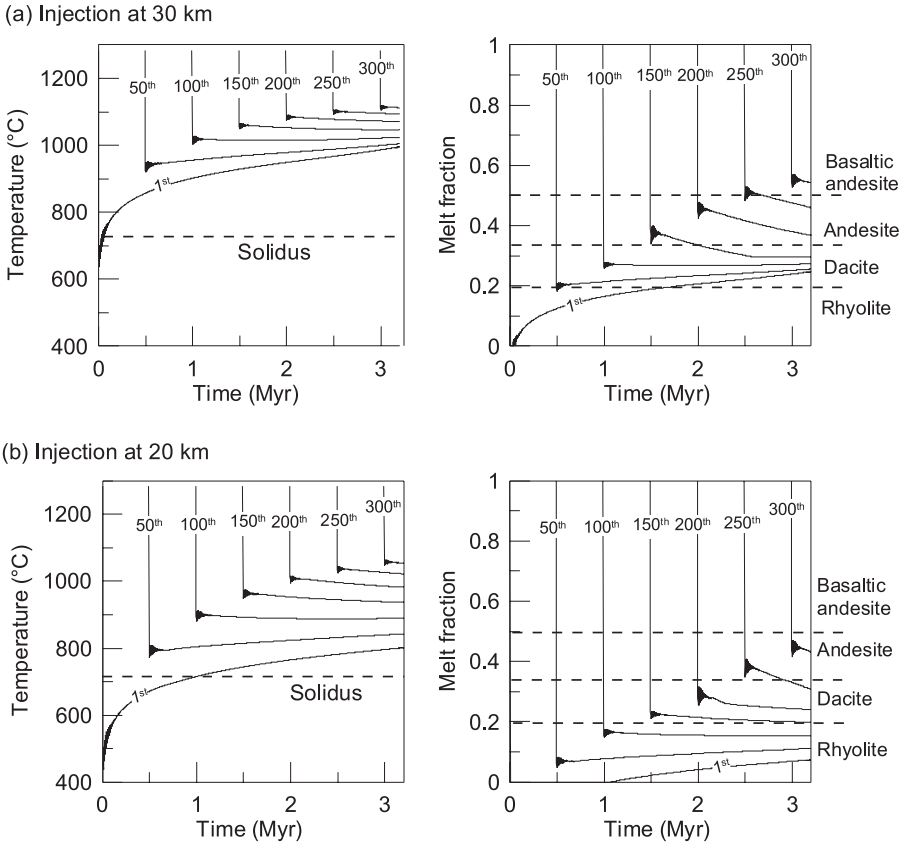

Fig. 7. Hot zone temperature (left) and melt fraction (right) evolution with time for a selection of basaltic sills injected into the lower crust. Sills 50 m thick are injected every 10 kyr, i.e. at an average emplacement rate of 5 mm/yr. The initial H_2O content of the basalt is 2·5 wt % and its injection temperature is 1285°C. The basalt is injected at a fixed depth of: (a) 30 km (Moho discontinuity); (b) 20 km (Conrad Discontinuity). The upper crust (above 20 km depth) is a pelite; the lower crust is amphibolite. The basalt cools very rapidly after injection to equilibrate thermally with the surrounding crust. Successive intrusions elevate the hot zone temperature. In the first tens of thousand years after injection, sill temperatures oscillate in response to the intrusion of subsequent sills. Eventually their temperature stabilizes when they are displaced sufficiently far below the injection level.

the system since the beginning of intrusions, whereas Fig. 11 shows the production rate, i.e. the amount of melt generated per unit of time. Figure 10a confirms that it is a lot more efficient to generate residual melt from the basalt at deep rather than at shallow level. For example, with an emplacement rate of 5 mm/year, after 3·2 Myr of basalt injection each 1 m of intruded basalt has generated 0·35 m of residual melt if emplaced at 30 km depth, 0·22 m if emplaced at 20 km depth, and only 0·14 m if emplaced at 10 km depth. If the sills are randomly emplaced in the lower crust, after 3·2 Myr, each 1 m of intruded basalt has, on average, generated 0·23 m of residual melt. Thus, to generate a given quantity of melt less basalt needs to be intruded at deep level than at shallow level.

The residual and crustal melt production rates strongly depend on the emplacement rate (Fig. 11). The production of residual melt continuously increases with time after the initial incubation period because more residual melt is generated with each new crystallizing basalt injection (Figs 10a and 11a). In contrast, the productivity of crustal melt is limited by the thickness of crust that can be partially melted. For a fixed intrusion depth, crustal melt productivity and production rates reach a maximum and then decrease (Figs 10b–d and 12b). This is because within the crust heat from the underlying basalt is transferred by conduction whereas the crust is cooled from above (fixed temperature at the Earth's surface). Thus the thickness of the partially melted crust is limited by heat diffusivity in the crust and cannot grow indefinitely. The situation is somewhat different for randomly emplaced sills because screens of crust are sandwiched between hot sills, thereby providing heating from below and above. Consequently, although it requires the longest incubation time, random sill injection is the most efficient way to partially melt the lower crust on a long timescale (Fig. 10b). Another efficient way to produce crustal melt is to inject basalt at 20 km in contact with a fertile upper crust (Fig. 10d). At still shallower depths the efficiency of this process is

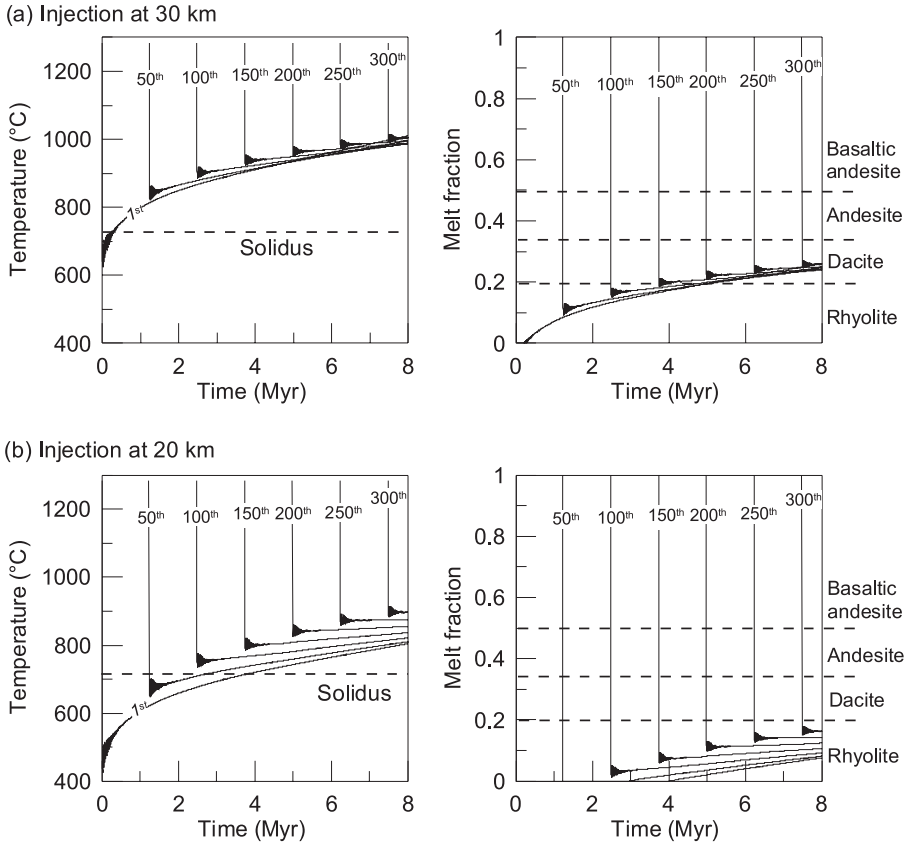

Fig. 8. Hot zone temperature (left) and melt fraction (right) evolution with time for a selection of basaltic sills injected into the lower crust. Basalt sills 50 m thick are injected every 25 kyr (average emplacement rate of 2 mm/yr) at (a) 30 km and (b) 20 km. The initial H_2O content, injection temperature and crustal compositions are as in Fig. 7. In this case the temperature in the hot zone grows more slowly than in Fig. 7 because of the lower emplacement rate; melt fraction (and composition) are more homogeneous.

diminished because of lower ambient temperatures (Fig. 10c and d).

Temporal and spatial controls on melt compositions

In the classical concept of evolved melt generation by basalt differentiation, a body of basalt slowly cools and crystallizes. The residual melt generated in this way becomes more evolved with time. In contrast, in our hot zone model the reverse is true: the system is heated with time as long as basalt continues to be injected. The formation of a residual melt from each rapidly cooling sill is instantaneous, but as the whole hot zone is heated, the generated melt becomes, on average, less evolved with time (Figs 7 and 8). The first residual melts to be produced in the hot zone correspond to the most silicic compositions (rhyolite) and lowest temperatures, evolving with time through dacite to andesite; a sequence opposite to that predicted by models of fractional crystallization in magma chambers. Only when basalts cease to be injected into the hot zone does the system cool and the sequence of melt evolution reverse.

Because sill temperature and melt fraction depend on their position on the geotherm, the compositional variation is also a function of depth. At any given time following the incubation period, a variety of residual and crustal melt compositions coexist across a range of depths in the hot zone (Figs 12–15). The shape of the geotherm and the consequent melt compositional diversity depend on the basalt emplacement rate. For example, in Figs 7 and 8 basalt is intruded with emplacement rates of 5 and 2 mm/year, respectively. After a total emplacement of 16 km of basalt at 30 km depth and an intrusion duration of 8 Myr, the melt fraction for an emplacement rate of 2 mm/year is 0·25–0·26, corresponding to dacitic melt compositions (Fig. 8). With an emplacement rate of 5 mm/year and after 3·2 Myr, which also corresponds to 16 km of intruded basalt, the melt fraction varies with depth from 0·25 to 0·54, corresponding to melt composition from dacite to basaltic andesite (Fig. 7). In the case of randomly emplaced intrusions, screens of amphibolite are sandwiched between basalt sills (Fig. 15).

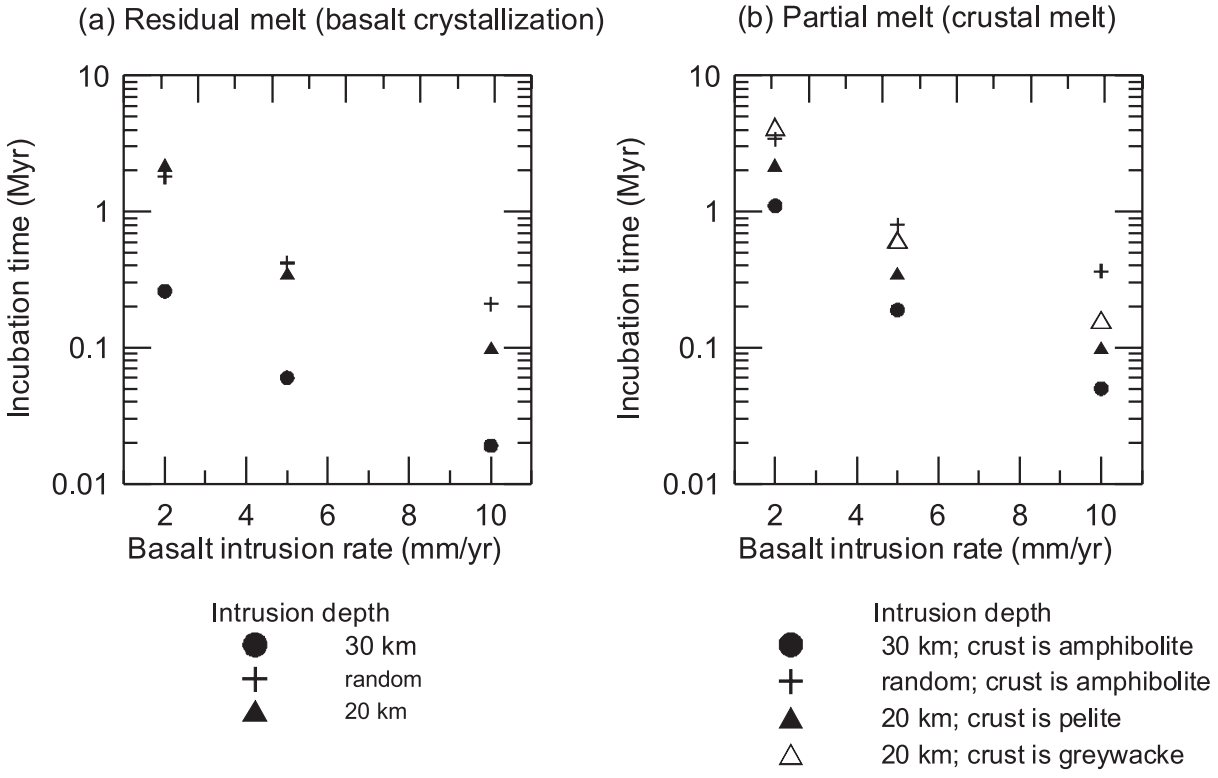

Fig. 9. Incubation time between the first intruded basalt and the beginning of melt accumulation for different average basalt emplacement rates and emplacement depths. (a) Residual melt; (b) crustal melt. The basalt initial H_2O content is 2·5 wt %, individual sill thickness is 50 m and the different emplacement rates correspond to different time intervals between intrusions.

At high temperature the amphibolite has a higher melt fraction than the basalt, whereas close to the solidus the melt fraction is higher in the basalt. Similarly, the ages of individual melts are spread out across the hot zone. In Figs 12–15, young melt that has differentiated from the last injected sill coexists with melts that were generated more than 3 Myr earlier. This has important implications for the apparent timescales of magmatic differentiation. In the likely case that melts from different depths within the hot zone are mixed together during ascent (e.g. Fig. 1), unravelling the timescales of differentiation from a single rock sample may be especially complicated.

Melt H_2O content

Basalt crystallization at high pressure concentrates H_2O in residual melts (Figs 12–14) even in the case where hydrous minerals such as amphibole are crystallizing. For relatively low melt fractions and high initial H_2O contents of the intruding basalt, the residual melt can be extremely H_2O-rich. For example, 65% crystallization of a basalt with an initial H_2O content of 2·5 wt % will lead to an andesitic residual melt with ~7 wt % H_2O. Elevated H_2O contents result in low melt viscosity and density (Figs 12–14). Thus, although the residual melt from basalt is rich in silica it is both buoyant and mobile. In contrast, the H_2O concentration of the crustal melt is limited by the H_2O content of the hydrated minerals in the protolith. As a consequence, crustal partial melts are much more viscous than the residual melts in the basalt (Figs 13d and 14d). This has implications for the relative extractability of crustal vs residual melts.

For low residual melt fractions in the basalt, the H_2O concentration can reach sufficiently high levels to become saturated, resulting in exsolution. This situation occurs if the parent basalt has more than ~1 wt % H_2O. Exsolved volatiles can flux the overlying crust and induce further melting. The transfer of H_2O from the basalt into the crust is difficult to constrain in low-porosity crust and we have, therefore, not explicitly modelled flux melting of the crust. For this reason, the amounts of crustal melt generated in our models should be considered as minima. H_2O exsolution may also enhance the extraction of melt by gas-driven filter pressing (Sisson & Bacon, 1999). Seismic observations are consistent with fluid exsolution and movement in the deep arc crust (Obara, 2002; Katsumata & Kamaya, 2003).

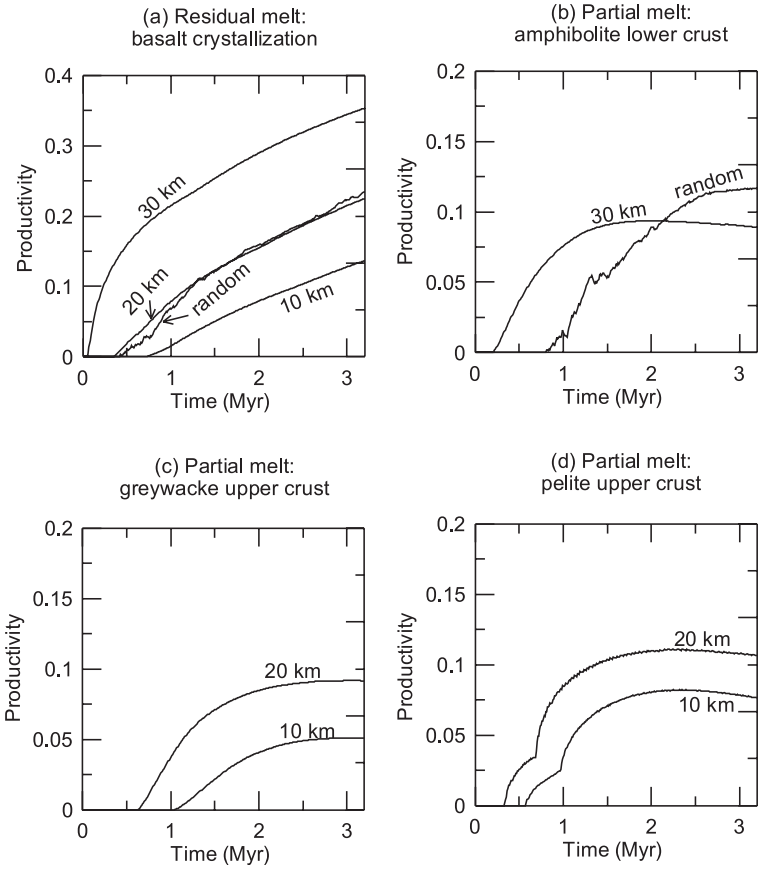

Fig. 10. Productivity for (a) residual melt from basalt crystallization, and crustal melts from: (b) amphibolitic lower crust; (c) greywacke upper crust; (d) pelite upper crust. Productivity is defined as the thickness of the accumulated melt divided by the total thickness of the intruded basalt. Basalt initial H_2O content is 2·5 wt %. One 50 m thick sill is injected every 10 kyr. Results are shown for fixed injection depths of 10, 20 and 30 km and for random intrusion between 20 and 30 km.

CONTRASTS BETWEEN DIFFERENTIATION IN DEEP HOT ZONES AND SHALLOW MAGMA CHAMBERS

Generation of evolved andesite and dacite melts in deep crustal hot zones can be contrasted with melt differentiation in shallow magma chambers. In the former case sills consolidate quickly and the evolved residual melt is generated on (geologically) short timescales. The residual melt can then be stored for long periods without further differentiation, because on a large scale the thermal profile of the hot zone evolves very slowly, on timescales governed by thermal conduction. In contrast, a shallow magma chamber requires high rates of magma input to be maintained in a molten state, as the surroundings are cold. Unless the heat input from the new magma input balances the heat loss from the chamber walls, then temperature and melt composition will evolve continuously. U-series data for evolved arc rocks commonly suggest that, following U–Th fractionation, magmas have residence times of the order of 10^4–10^5 years (Reagan *et al.*, 2003; Zellmer *et al.*, 2003*b*). We suggest that such long residence times are hard to reconcile with a shallow magma storage system because of the requirement of stable thermal conditions. In a deep hot zone the residual melt is stored at temperatures governed by the geotherm, allowing melt to remain compositionally stable for long periods.

The high H_2O content of residual melts also has important implications for their physical properties, specifically reduced density and viscosity, which mean that melts can be readily concentrated by compaction, facilitating extraction, and rapid ascent toward the surface. Carmichael (2002) arrived at a similar conclusion regarding the H_2O-rich andesites of the Mexican volcanic arc. He argued that their low viscosity and density allowed magma ascent to be near-adiabatic. The adiabat for hydrous andesite melts is of the order of 25–50°C/GPa (Mastin & Ghiorso, 2001; Carmichael, 2002). Consequently, there may be only 50–100°C difference

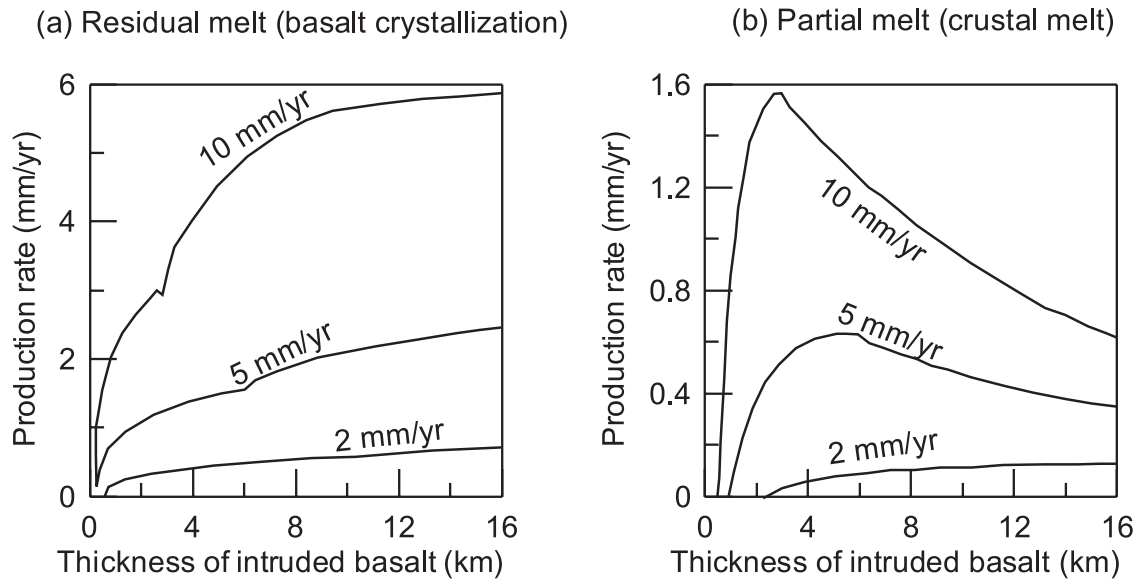

Fig. 11. Melt production rates (mm/yr) for different basalt intrusion rates (2, 5, 10 mm/yr), for (a) residual melt, and (b) crustal melt as a function of the thickness of the intruded basalt. The production rate is defined as the thickness of melt generated per year. The basalt emplacement depth is 30 km. The curves were smoothed to eliminate peaks caused by model discretization.

between andesite generation temperatures in the lower crust and low-pressure equilibration temperatures inferred from mineral thermometry or phase equilibria.

A further implication of our model is the significant thickening of the crust that results from basalt emplacement. If melt is efficiently extracted then the residual basalts will have a cumulate character, with associated high densities and seismic velocities, as observed in exposed deep crustal sections through arcs (Debari & Coleman, 1989). In some cases, the processes of delamination and recycling of dense mafic cumulates in the less dense underlying mantle can be invoked to limit the extent of crustal thickening (Kay & Kay, 1993; Jull & Kelemen, 2001). In the Sierra Nevada, USA, for example, seismic refraction and gravity data (Fliedner *et al.*, 1996, 2000) show that the granitic rocks of this young mountain belt are not supported by an isostatic root, which Fliedner *et al.* (1996, 2000) attributed to delamination of the mafic counterpart to the granites. Such an interpretation is consistent with rapid Pliocene uplift in the region and the change in the petrology of xenoliths in basalt lavas from predominantly lower crustal granulites to predominantly mantle peridotites between 10 and 3 Ma (Ducea & Saleeby, 1996, 1998*a*, 1998*b*; Ducea, 2002; Farmer *et al.*, 2002). A more recent seismic experiment across the southern Sierra Nevada, by Zandt *et al.* (2004), using receiver functions, has identified a welt of thickened crust and a 'hole' in the Moho, which those workers ascribed to asymmetric flow of dense lower crust into a delaminating mantle drip beneath the Great Valley. In other arcs, for which there is less compelling evidence for delamination, the apparent lack of a deep cumulate root may simply be a consequence of the difficulty of seismically distinguishing pyroxenites and/or garnet-rich mafic rocks from mantle peridotite. For example, Fliedner & Klemperer (2000) proposed that beneath the Aleutians volcanic arc some 10 km of ultramafic cumulates lie below the geophysical Moho.

MELT SEGREGATION

The storage of evolved residual melts in the deep crustal hot zone depends critically on the dynamics of cooling and crystallization of each sill. Two end-member scenarios can be envisaged, and mirror observations of differentiation in high-level intrusions. In one end-member the magma body retains its suspended crystals and consolidates as a physically undifferentiated layer of partially molten rock. Crystallization is near equilibrium and porous media processes are required to segregate the evolved residual melts. In the other end-member, crystals and melt are efficiently separated during cooling; for example, by crystal settling and floor crystallization with compositional convection (Tait *et al.*, 1984). The sill thus becomes strongly physically differentiated and evolution may be closer to fractional crystallization. In either case the sill may, in principle, develop into a lower layer of cumulates and an upper layer of buoyant crystal-free evolved residual melt, which may detach immediately or shortly after sill consolidation. Studies of shallow sills suggest that both these end-members, and intermediate situations, can occur depending on many parameters, including sill thickness, density and viscosity of melt, and whether convection develops.

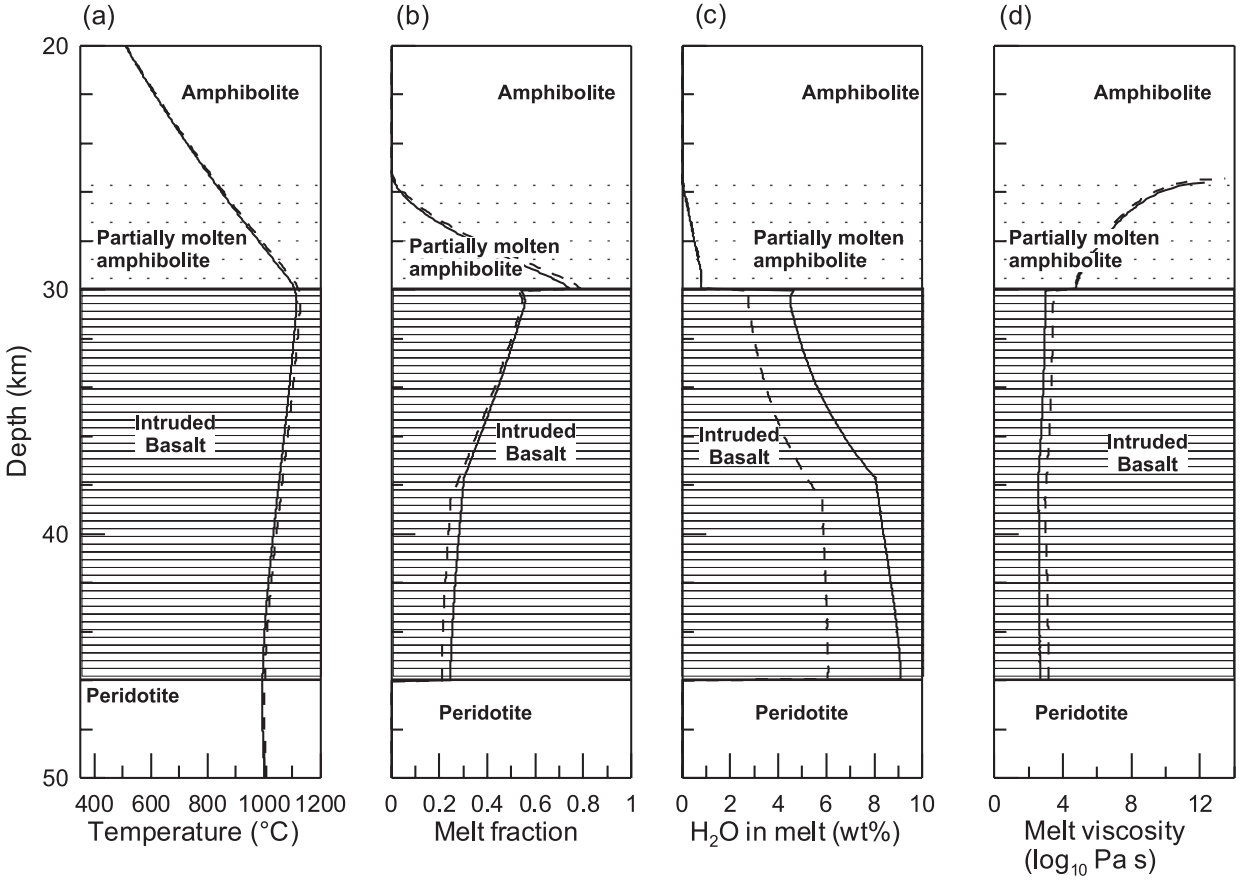

Fig. 12. Variation of (a) temperature, (b) melt fraction, (c) melt H_2O content, and (d) melt viscosity as a function of depth, taken as a snapshot 3·2 Myr after initiation of the hot zone shown in Fig. 7a. The total added thickness of intruded basalt at this stage is 16 km; the original crustal thickness was 30 km. Melt viscosity is calculated using the equation of Baker (1998). Continuous line shows basalt with initial H_2O content of 2·5 wt % and an injection temperature of 1285°C; dashed line shows basalt with initial H_2O content of 1·5 wt % and injection temperature of 1302°C. The amphibolite lower crust has become partially melted. Its melt fraction is high but its H_2O content is low because of low initial H_2O content. Thus, the viscosity of the crustal melt is high compared with the viscosity of the H_2O-rich residual melt.

Several mechanisms have been proposed for the segregation of buoyant partial melts; namely, compaction of partially molten rock, large-scale Rayleigh–Taylor instabilities of the entire hot zone, and tectonic deformation. The rate of segregation by compaction is very sensitive to melt viscosity (McKenzie, 1985). The high H_2O content of hot zone residual melts will result in low viscosity (Figs 12–14) and low density (<2300 kg/m^3). For a typical viscosity of 10^3 Pa s compaction-driven segregation times are estimated to be in the range 10^4–10^6 years for a porosity of the order of 10% (McKenzie, 1985). Long residence times of evolved melts in the deep crust are consistent with data from studies of $^{230}Th/^{226}Ra$ disequilibrium in many intermediate and silicic arc volcanic rocks (Reagan *et al.*, 2003; Zellmer *et al.*, 2003*b*).

Jackson *et al.* (2003) coupled heat transfer from basaltic sills, partial melting of crustal rocks and melt segregation by compaction processes. Their model focuses on the segregation of partial melts from heated crustal rocks, but the same principles can be applied to residual melts in basaltic sills. Melt segregates to produce porosity waves, which move upwards because of buoyancy and start to accumulate at depths just above the solidus. Unmelted rocks above the depth at which the solidus is reached are considered impermeable, so melt cannot ascend by compactional mechanisms. Thus the depth in the crust at which the geotherm reaches the solidus temperature is highly significant, because residual melts from basalt and partial crustal melts can only exist below this depth. Jackson *et al.* (2003) also showed that segregated melts in high-porosity zones can have the geochemical attributes of highly evolved melts.

Melts can segregate more rapidly when the partially molten rock is deformed (Petford, 2003). Tectonic processes and large-scale Rayleigh–Taylor buoyancy instabilities in the entire hot zone can cause deformation and melt segregation (De Bremond d'Ars *et al.*, 1995). Interaction between extracted melts from one layer and

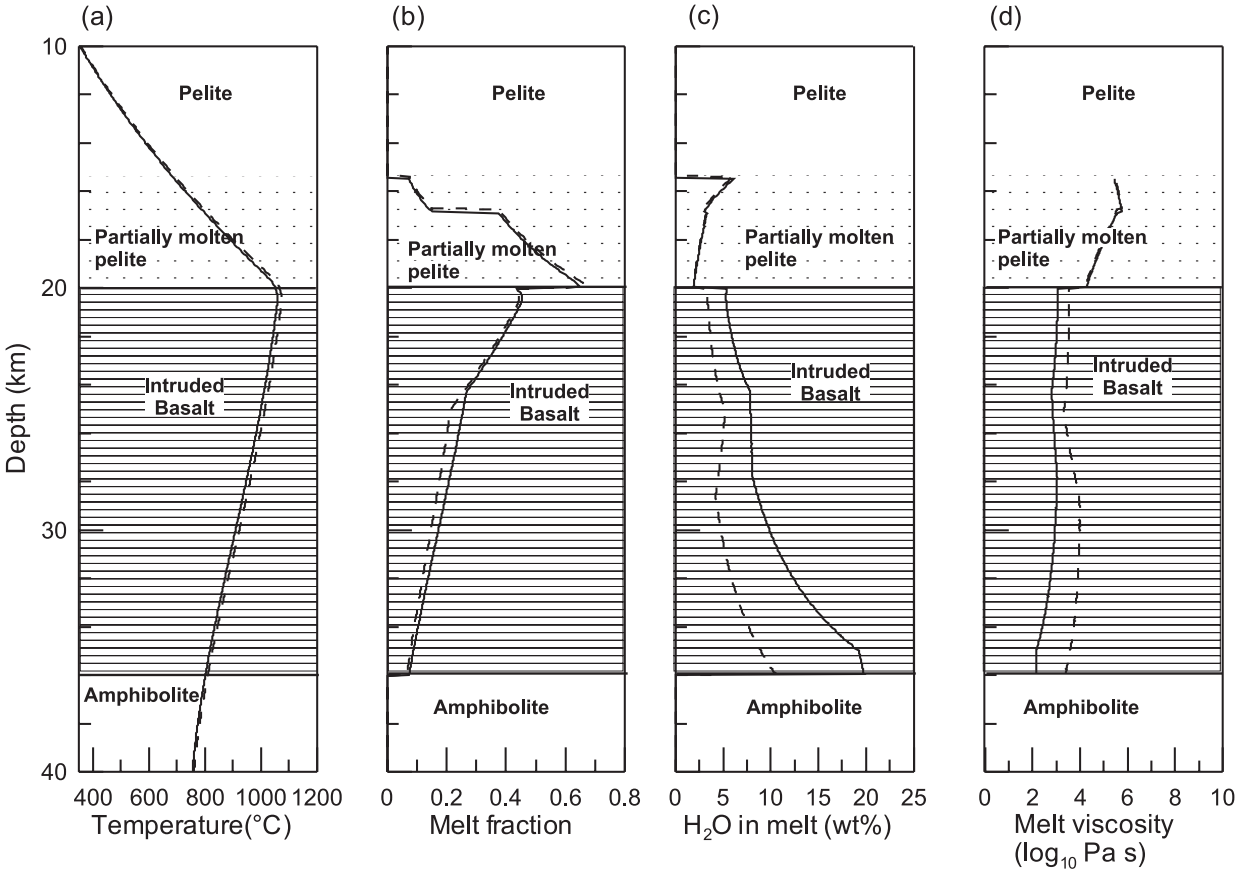

Fig. 13. Variation of (a) temperature, (b) melt fraction, (c) melt H_2O content, and (d) melt viscosity as a function of depth, 3·2 Myr after initiation of the hot zone shown in Fig. 7b. The total added thickness of basalt, original crustal thickness and melt viscosity are as in Fig. 12. Continuous line shows basalt with initial H_2O content of 2·5 wt % and an injection temperature of 1285°C; dashed line shows basalt with initial H_2O content of 1·5 wt % and injection temperature of 1302°C. The pelitic upper crust has become partially melted. The low H_2O initial content of the pelitic melt accounts for the low viscosity of the crustal melt relative to the H_2O-rich residual melt. Saturation of the melt in H_2O is reached at the base of basalt column. Saturation values are taken from Zhang (1999).

melts from other layers, with lower or higher melt fractions, will result in chemical mixing between more and less evolved melts, leading to a wide spectrum of melt compositions extracted from the hot zone (e.g. Fig. 1). These hybrid melts should define linear chemical trends in contrast to the curved trends diagnostic of fractional crystallization alone.

PETROLOGICAL CONSTRAINTS ON THE ASCENT OF ANDESITE MELT

We now consider the ascent of evolved residual melts segregated from a deep hot zone. This exercise requires information on the liquidus temperature (T_L) of a particular andesite composition as a function of H_2O content from pressures between those of the lower crust and the depth of H_2O saturation. Unfortunately, to date, no such study has been carried out experimentally, and the desired information can only be compiled for a range of experimental studies, and must be considered semi-quantitative.

Figure 16 shows the liquidus surface, contoured for H_2O content, of a typical silicic andesite. This was constructed from available phase equilibria experiments in which the residual melt composition was within 2 SD of the average 1980–1986 Mount St. Helens silicic andesite for the components SiO_2, Al_2O_3, MgO, FeO, CaO and $Na_2O + K_2O$ (see Fig. 16 caption for average values). We assume that the minor components TiO_2, MnO and P_2O_5 have negligible effect on phase relations. We have also used some experimental data from older near-liquidus experimental studies (e.g. Eggler, 1972; Green, 1972) in which the residual melt composition was not analysed, but where the starting composition is within 2 SD of the Mount St. Helens average. Our approach involves a number of approximations. We assume that fO_2 has only a small effect on phase relations, which is not strictly true for amphibole (Allen & Boettcher, 1983;

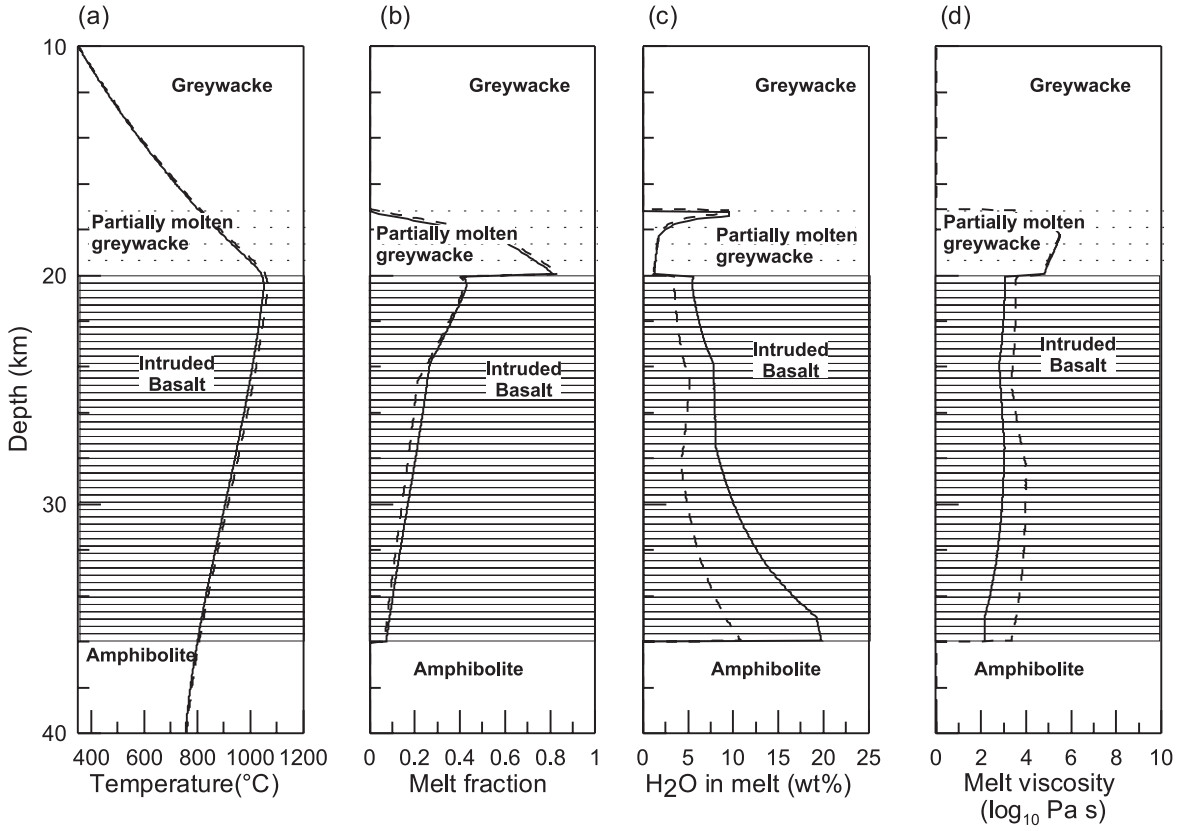

Fig. 14. Variation of (a) temperature, (b) melt fraction, (c) melt H_2O content, and (d) melt viscosity as a function of depth, 3·2 Myr after initiation of the hot zone. In contrast to Fig. 13, the basalt is injected at 20 km in contact with a greywacke upper crust. The total added thickness of intruded basalt, original crustal thickness and melt viscosity are as in Fig. 12. Continuous line shows basalt with initial H_2O content of 2·5 wt % and an injection temperature of 1285°C; dashed line shows basalt with initial H_2O content of 1·5 wt % and injection temperature of 1302°C. The greywacke upper crust has become partially melted. Saturation of the melt in H_2O is reached at the base of basalt column. Saturation values are taken from Zhang (1999).

Rutherford & Devine, 1988). However, all of the experiments we have used were conducted within 2 log units of the NNO (nickel–nickel oxide) buffer, which reduces the impact of this assumption. Because oxide stability is closely linked to fO_2, we have not shown the stability field of oxide minerals (magnetite and ilmenite) in Fig. 16. Another assumption is that small differences in melt chemistry (i.e. within 2 SD of the average dacite) also have little effect on phase relations. Finally, we have had to use a variety of methods to estimate the dissolved H_2O content of quenched melts (see Fig. 16 caption for details), which imparts absolute uncertainties of approximately ±1–2 wt % to the contours of 10, 7 and 5 wt % H_2O in Fig. 16.

An important feature of Fig. 16 is the curvature of the liquidi for melts with fixed H_2O content. At high pressures, well above H_2O saturation, these liquidi are straight and lie parallel to the anhydrous liquidus. The curvature of the liquidi as they approach the H_2O-saturated liquidus at low pressure is consistent with experiments on haplogranite (Johannes & Holtz, 1990) and natural granite (Whitney, 1988). In Fig. 17 we show that this configuration, which has important implications for magma ascent, is consistent with the experimentally determined liquidus of the 1991 dacite of Mount Pinatubo with dissolved H_2O contents of 7·1 ± 0·5 wt %, at pressures of 220–960 MPa (Rutherford & Devine, 1988; Scaillet & Evans, 1999; Prouteau & Scaillet, 2003).

Figs 16 and 17 differ fundamentally from conventional phase diagrams, which represent the equilibrium mineral assemblage for a given bulk-rock composition with a fixed H_2O content. Although the bulk composition remains constant across such a phase diagram, the melt composition changes continuously from the liquidus to the solidus. In contrast, the liquidus surface diagrams in Figs 16 and 17 apply to a single liquid composition with various amounts of dissolved H_2O. The mineral phases shown in the diagram are those that crystallize at the liquidus; subliquidus phase relations cannot be represented. Liquidus phases vary with pressure, temperature, and dissolved H_2O. Amphibole is stable only for H_2O contents

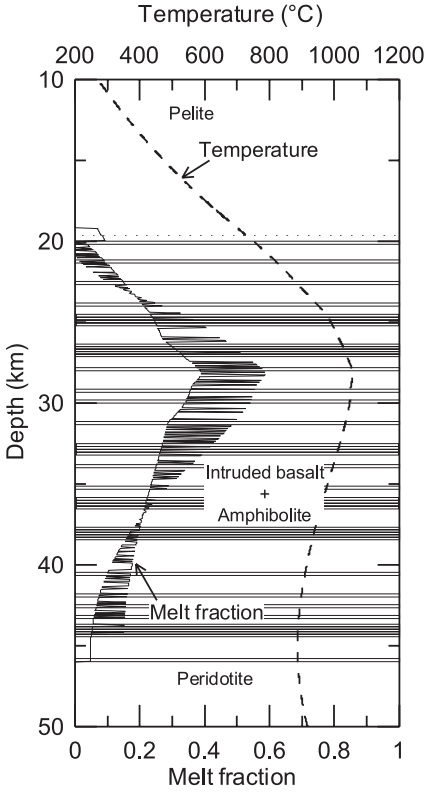

Fig. 15. Variation of melt fraction and temperature as a function of depth for a hot zone formed by sills randomly injected in the lower crust between the Conrad Discontinuity and the Moho. The continuous line denotes melt fraction (lower abscissa); the dashed line denotes temperature (upper abscissa). Basalt initial H_2O content is 2·5 wt % and injection temperature is 1285°C. Basalt sills of 50 m thickness were emplaced every 10 kyr. On the melt fraction curve, high melt fraction peaks alternate with lower melt fraction screens. Below about 950°C, the high melt fraction peaks correspond to basalt sills and the lowest melt fractions correspond to screens of lower crust sandwiched between basalt sills. At higher temperature the amphibolite becomes more fertile than the basalt (Fig. 5b) and the reverse is true. The upper crust is pelite and is also partially melted.

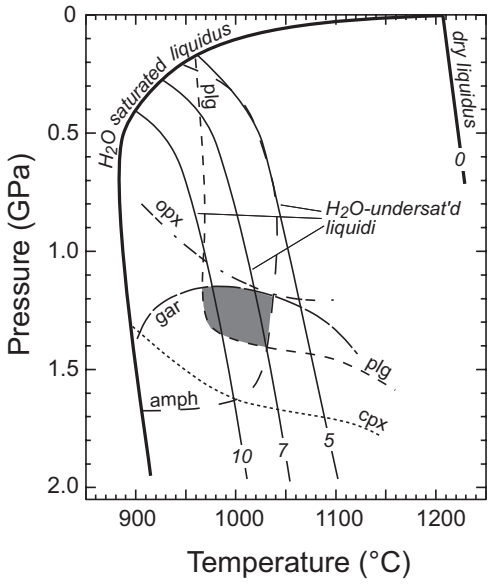

Fig. 16. Pressure–temperature diagram showing liquidus surface for a silicic andesite contoured for 5, 7 and 10 wt % dissolved H_2O. Liquidus and near-liquidus fields for plagioclase, amphibole, garnet, orthopyroxene and clinopyroxene are delineated with dashed lines, labelled on their stable side. The stability field of liquidus oxides is omitted for clarity. The field of residual garnet amphibolite is shaded. The diagram was compiled using all available published data for experimental liquids (glasses) whose compositions lie within 2 SD of the mean composition of silicic andesite erupted from Mount St. Helens over the period 1980–1986 (i.e. 63·3 ± 1·7 wt % SiO_2; 0·65 ± 0·06% TiO_2; 17·7 ± 0·6% Al_2O_3; 4·4 ± 0·5% FeO; 2·1 ± 0·4% MgO; 5·2 ± 0·6% CaO; 4·7 ± 0·2% Na_2O; 1·3 ± 0·2% K_2O; n = 76). At pressures below 0·4 GPa the phase equilibria are taken from experimental data on Mount St. Helens itself [as summarized by Blundy & Cashman (2001)]. At higher pressures 37 experimental runs on different starting materials from the following sources were used: Green & Pearson (1985), seven runs; Kaszuba & Wendlandt (2000), two runs; Kawamoto (1996), 10 runs; Nicholls & Harris (1980), seven runs; Johannes & Koepke (2001), one run; Green (1992), one run; Müntener *et al.* (2001), two runs; Carroll & Wyllie (1990), three runs; J. D. Blundy & R. Brooker (unpublished data, 2000), one run; Sen & Dunn (1994), one run; Rapp & Watson (1995), one run; Allen & Boettcher (1983), one run. The slope of the dry liquidus is taken from Eggler & Burnham (1973). H_2O contents of melts were estimated by several methods. Where the glass composition is taken from electron microprobe analyses of an experimental product, we used the volatiles by difference method, which can be unreliable (accuracy ±1–2 wt % H_2O). Where the experiment was a near-liquidus run on a suitable starting material, we used the H_2O initially added to the experimental capsule, assuming negligible H_2O loss from the capsule and little effect from the small amount of crystallization. For H_2O-saturated near-liquidus experiments we estimated the H_2O solubility at the appropriate pressure and temperature (Newman & Lowenstern, 2002). Finally, in the case of three experimental glasses (Müntener *et al.*, 2001; J. D. Blundy & Brooker, 2004) (unpublished data, 2000) H_2O was determined directly and accurately by ion-microprobe.

≥4 wt % (Eggler, 1972) and temperatures below ~1050°C, the maximum temperature at which liquids of andesite composition can be in equilibrium with amphibole (e.g. Müntener *et al.*, 2001). Orthopyroxene is confined to relatively low pressures and temperatures over 920°C, whereas garnet appears only above ~1·1 GPa. Clinopyroxene has a wide field of liquidus stability, although its presence is sensitive to the CaO content of the bulk liquid. Plagioclase stability decreases and *An* content increases with increasing pH_2O. Based on the experimental data of Kawamoto (1996) and Pichavant *et al.* (2002*b*) we infer that the maximum H_2O content of andesite melts in equilibrium with plagioclase ($An_{>80}$) is ~10 wt % H_2O.

Figure 16 can be used to constrain the residual mineralogy of the source rocks from which a silicic andesite could be produced either by crystallization in a deep crustal hot zone or by partial melting of the lower crust. A broad stability field for amphibolite (± garnet) is defined, confirming the viability of producing andesites with ≥6 wt % H_2O in a lower crustal hot zone.

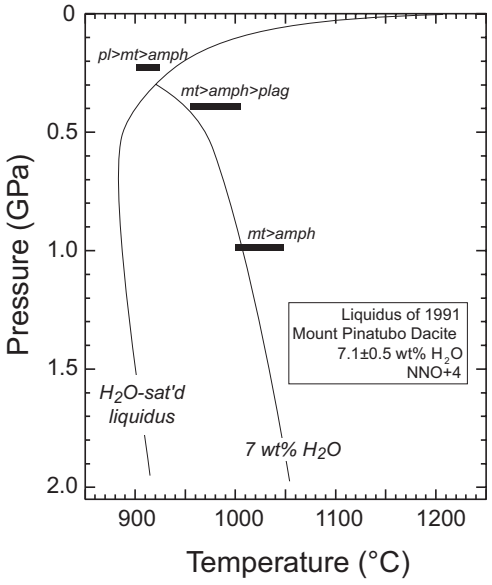

Fig. 17. Pressure–temperature diagram showing liquidus surface of Mount Pinatubo dacite with 7·1 ± 0·5 wt % H_2O, $fO_2 \approx$ NNO + 4, and pressures of 0·4 and 0·96 GPa (Prouteau & Scaillet, 2003) and 0·23 GPa (Scaillet & Evans, 1999). Horizontal bars extend from the sub-liquidus experimental temperature (X >0·8) to the extrapolated liquidus (see Prouteau & Scaillet, 2003, fig. 1). Labels denote liquidus phases in order of appearance. The H_2O-saturated liquidus and liquidus with 7 wt % H_2O are taken directly from Fig. 16 and show good agreement with the Mount Pinatubo data. The slightly lower H_2O-saturated liquidus temperature of Mount Pinatubo dacite relative to Fig. 16 is a consequence of its slightly higher SiO_2 content (64·6 wt % compared with 63·3 wt %).

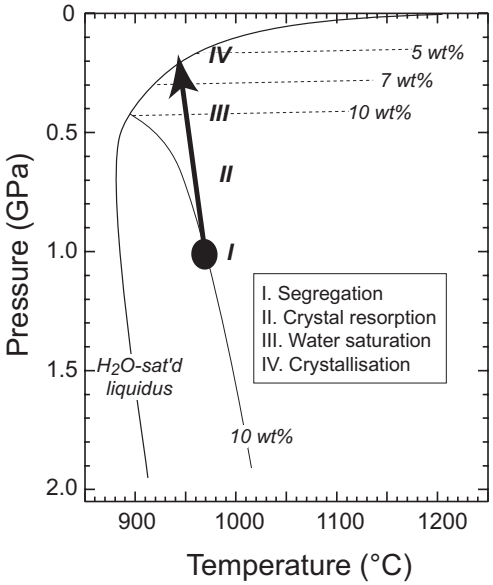

Fig. 18. Pressure–temperature diagram showing the proposed ascent path for a silicic andesite melt with 10 wt % H_2O generated at 1 GPa and 970°C, indicating processes taking place at different stages of magma ascent (I–IV). The liquidi for a melt that is H_2O-saturated and one that contains 10 wt % dissolved H_2O are taken from Fig. 16. The melt is assumed to ascend adiabatically with cooling of ~40°C/GPa (Holtz & Johannes, 1994). Immediately after melt segregation (I), the melt temperature exceeds that of the liquidus and the melt becomes superheated (Clemens *et al.*, 1997). Any entrained source crystals (restite or cumulates) or accidentally incorporated xenolith material may be resorbed at this stage (II), which will lead to *pro rata* magma cooling (not shown). The melt attains H_2O saturation at ~0·4 GPa (III) at a temperature still above the liquidus (assuming no resorption-related cooling). H_2O exsolution is therefore not accompanied by crystallization at this stage. Crystallization begins (IV) when the melt intersects the H_2O-saturated liquidus at ~0·22 GPa. At this stage melt, containing only ~6 wt % H_2O, may become trapped as inclusions in growing phenocrysts. Subsequent ascent will involve further degassing and crystallization and will therefore leave the compositional plane of the diagram.

MELT ASCENT, DEGASSING AND CRYSTALLIZATION

The low viscosity and density of H_2O-rich andesite and dacite residual melts produced at temperatures of 850–1050°C (Figs 12–14) suggest that their ascent may be rapid, most probably along dykes, and, therefore, on timescales that are much shorter than melt storage times (Petford *et al.*, 2000). Rapid magma ascent will approach adiabatic conditions, with cooling of 25–60°C/GPa over the pressure range 1·0–0·3 GPa (Holtz & Johannes, 1994; Clemens *et al.*, 1997; Carmichael, 2002). An adiabatic ascent path from a source rock at nominal conditions of 970°C and 1 GPa (equivalent to ~34 km depth in the crust) is illustrated in Fig. 18. Under these conditions the melt has ~10 wt % dissolved H_2O, which is insufficient to saturate it at this pressure. Because the adiabat has a slightly steeper slope than the liquidus for 10% H_2O, immediately after leaving the source region the melt can become superheated (Holtz & Johannes, 1994; Clemens *et al.*, 1997). This will be true of any H_2O-undersaturated melt because the liquidus curves at constant H_2O are near parallel (Fig. 16) and the adiabatic gradient is weakly dependent on dissolved H_2O content. Any entrained source material, such as restite (Chappell & White, 2001) in the case of partial melting, or cumulates in the case of crystallization, will be partially or wholly dissolved. Some of the ubiquitous, highly corroded plagioclase phenocryst cores of silicic calc-alkaline rocks may originate in this way. The effect of cumulate or restite resorption will impart linear chemical trends to the rocks that will be hard to distinguish from magma mixing. Xenocrystic materials from the wall-rocks can also be melted, providing a mechanism of open-system behaviour, as required by Sr isotope profiles across complexly zoned and resorbed plagioclase crystals in andesites (Davidson *et al.*, 2005). The extent of melting or dissolution depends on a combination of thermodynamic and kinetic factors. Thermodynamic control is related to the maximum potential superheat (i.e. the separation between adiabat and liquidus in Fig. 18) and the latent heat of

fusion. Kinetic control depends on the ascent rate and the time available for dissolution, which is ultimately limited by diffusion in the melt. Melting and dissolution will result in cooling of the magma and consumption of superheat.

After the resorption phase of ascent, a melt with 10 wt % H_2O becomes H_2O-saturated at ~0·4 GPa (~14 km depth). If the melt retains superheat, degassing of H_2O need not, at this stage, be accompanied by crystallization (Fig. 18), although some cooling of the melt will occur as a result of adiabatic expansion of exsolved gas (~15°C per % of gas exsolved). Knowledge of magma volatile contents comes from studies of melt inclusions in phenocrysts (Anderson, 1979; Cervantes & Wallace, 2003). To trap inclusions, the magma must undergo crystallization. Thus, the original high H_2O contents may not be preserved in melt inclusions, which are unlikely to form until the melt intersects the H_2O-saturated liquidus and begins to crystallize. In our example H_2O-saturated crystallization begins at 0·2 GPa (7–8 km depth), when the dissolved H_2O content has decreased to 5–6 wt % (Fig. 18). Thus, melt inclusions will record only a minimum pre-eruptive H_2O content (in this case 5–6 wt %), even though the original H_2O content was considerably higher. Melts can also undergo significant degassing of other volatile species (e.g. SO_2, CO_2) in addition to H_2O long before they become trapped as melt inclusions. This has implications for the 'missing' budget of some magmatic volatiles (e.g. SO_2; Wallace, 2001) based on the discrepancy between field estimates of volatile emission at active volcanoes and petrological estimates of volatile contents integrated over the erupted volume.

Initial crystallization of andesite at the H_2O-saturated liquidus involves amphibole or pyroxenes, depending on bulk composition and H_2O content. Subsequent crystallization will be dominated by plagioclase, the proportion of which increases with decreasing pressure (Fig. 3). As pressure decreases there will be a concomitant decrease in the *An* content of plagioclase from a maximum value at the initial point of saturation. Amphibole eventually becomes unstable at pressures less than ~0·1 GPa (Rutherford & Hill, 1993) and will either become resorbed or be pseudomorphed by anhydrous reaction products. The exact breakdown pressure of amphibole is sensitive to temperature and the SiO_2 content of the melt; amphibole persists to lower pressure at lower temperature and/or in more evolved melts (Sato *et al.*, 1999). After reaching the H_2O-saturated liquidus, a large amount of crystallization occurs over a relatively small pressure drop. Using available experimental data, Blundy & Cashman (2001) showed that for an H_2O-saturated silicic andesite at 900°C, crystal content increases by 29% from 240 MPa (7–8 km) to 125 MPa (3–5 km), i.e. an isothermal crystallization rate of 0·23%/MPa. The corresponding crystallization rates for Colima andesite at 955°C and Mont Pelée andesite at 925°C are 0·34%/MPa (Fig. 3a) and 0·08%/MPa (Martel *et al.*, 1999), respectively. Decompression crystallization rates will be slightly greater if adiabatic expansion and H_2O exsolution are taken into account. However, in rapid magma ascent, crystallization and degassing can be delayed by kinetic effects. For example, supersaturation overpressures of tens of megapascals are required for homogeneous bubble nucleation (Navon & Lyakhovsky, 1998). The onset of strong degassing could be sudden, inducing strong undercooling and rapid crystallization in the upper crust. Such conditions might also be conducive to trapping melt inclusions in rapidly growing phenocrysts.

Table 2: Calculations for the transport of hydrous andesite magmas through dykes in the crust

Pressure (MPa)	Depth (km)	X	$\log(\mu_{melt})$ (Pa s)	$\log(\mu_{magma})$ (Pa s)	H_2O (wt %)	v_{ascent} (m/h)	Time
380	15	1·00	3·0	3·0	8	792	0
290	11·4	0·88	3·63	3·88	7	108	14 h
214	8·4	0·75	4·34	4·92	6	9·4	5·6 days
149	5·8	0·62	4·88	5·97	5	0·84	7·7 weeks
95	3·7	0·55	5·70	7·20	4	0·05	1·1 years

Melt initially contains 8 wt % H_2O and becomes H_2O saturated at 380 MPa. X, melt fraction; μ_{melt} and μ_{magma}, melt viscosity and magma viscosity, respectively; v_{ascent}, ascent velocity; Time, time elapsed since the magma reached H_2O saturation. (See text for details of the calculations.)

The combined effect of decreasing H_2O content and increasing crystal content increases magma viscosity considerably, which has major implications for magma ascent. We illustrate this with some representative calculations for an andesite melt with a temperature of 900°C and 8 wt % H_2O that reaches its H_2O-saturated liquidus at 380 MPa (see Fig. 18), equivalent to a crustal depth of ~15 km. We estimate the viscosity of the melt as it ascends adiabatically to a pressure of 95 MPa and temperature of 860°C with decompression crystallization rates of 0·13–0·20%/MPa, consistent with experimental studies. We assume that the melt phase evolves from andesite to rhyolite as it crystallizes and that the water content of the melt varies according to Henry's law with a solubility coefficient of $4{\cdot}1 \times 10^{-6}$ per Pa (Newman & Lowenstern, 2002). We estimate melt viscosity as a function of temperature, H_2O content and composition using experimental data (Dingwell *et al.*, 1998) and take account of the effect of suspended crystals on viscosity using the empirical relationship of Marsh (1981).

Table 2 shows the results of our model calculations. Melt viscosity increases by 2·7 orders of magnitude,

whereas magma (melt + crystals) viscosity increases by 4·2 orders of magnitude over the depth range from 15 to 3·7 km. The changes are strongly non-linear because of the combined effects of degassing, changing melt composition and crystal growth. The rapid increase in viscosity during decompression crystallization is in contrast to the previous 25 km or so of transport from the deep crustal hot zone, during which crystal fraction was negligible, and viscosity and density remained very low and approximately constant. The net effect is that the magma's resistance to flow increases substantially as it enters the shallow crust.

The consequences of increasing magma viscosity on ascent rate and ascent time can be estimated with reference to current understanding of dyke propagation (Lister & Kerr, 1991; Rubin, 1995; Menand & Tait, 2002). A pressure P_e is required to open a dyke of width $2w$ over a horizontal length b by the following relationship:

$$w = 2bP_e(1-\nu^2)/E \quad (7)$$

where ν is Poisson's ratio and E is the elastic modulus. We assume that the overpressure is constant at 10 MPa, consistent with estimates of magma pressure in andesite eruptions (Stasiuk *et al.*, 1993). We assume that the dyke width is 2 m ($w = 1$ m) by choosing $\nu = 0{\cdot}3$, $E = 3{\cdot}64 \times 10^{10}$ Pa and $b = 1000$ m. We further assume that the vertical propagation velocity of the dyke is controlled by the balance between overpressure and viscosity, μ:

$$u = P_e w^2/3\mu l \quad (8)$$

where l is the vertical distance between the dyke tip and the source, which we assume is in the hot zone at a depth of 30 km. The calculated velocities are listed in Table 2 along with the times at which the magma reaches a given depth after onset of H_2O-saturated crystallization at 15 km. The calculations shows that wet andesite magmas will slow down dramatically in the shallow crust. When the timescale of ascent becomes longer than the timescale of conductive cooling of the dyke the magma will cease to ascend, a process we refer to as 'viscous death'. For the example in Table 2, the timescale of conductive cooling is estimated to be of the order of 20 days (taking $\tau \sim w^2/\kappa$, where κ is the thermal diffusivity, taken to be 5×10^{-7} m^2/s). Thus in this particular case the dyke experiences viscous death at ~6–7 km depth. The timescales can also be compared with experimental investigations of crystallization and kinetics in silicic melts (Hammer & Rutherford, 2002; Couch *et al.*, 2003), which indicate that kinetic timescales are several hours to days in andesitic systems. Thus, the deeper parts of the ascent path could be sufficiently fast that significant undercoolings develop. The ascending magma may, therefore, miss out entirely on the high-pressure stage of decompression crystallization.

With different parameter values [e.g. larger dyke width and/or overpressures in equation (7), shallower source in equation (8), and higher magma temperature] faster ascent velocities and wider dykes are implied, increasing the chances of the magma reaching near the Earth's surface, and increasing the chances of strong undercooling developing and low-pressure crystallization being dominant. Conversely, most magmas ascending and crystallizing as a result of decompression would be expected to stall at depths of 4–10 km, and, thereafter, cool and crystallize to form granite plutons. It is therefore likely that the emplacement depth of granite magmas is strongly controlled by the dissolved H_2O content in the magma as it leaves its source region. Our calculated stalling depth (or viscous death) is in good agreement with the typical emplacement depth of granite bodies (e.g. Hammarstrom & Zen, 1986; Hollister *et al.*, 1987; Anderson & Smith, 1995). Hotter and drier magmas are expected to be emplaced at shallower levels in the crust than cooler wetter magmas, all other transport parameters (dyke width, overpressures, etc.) being equal.

These ideas can be extended to consider the evolution of shallow magma chambers and granite plutons. We envisage that evolved magmas generated in the hot zone are extracted in pulses (see Bons *et al.*, 2004), the frequency of which is related to the timescales of melt segregation processes. Once detached from its source each pulse ascends rapidly into the shallow crust, where it stalls as a result of decompression crystallization. Shallow magma chambers and granite plutons grow by the amalgamation of numerous such magma pulses (John & Blundy, 1993; Glazner *et al.*, 2004). The same principles of heat advection that control the development of a lower crustal hot zone apply to magma pulses emplaced into the upper crust. If the magma supply rate is sufficiently fast then heat is advected into the upper crust at a faster rate than it can be extracted by cooling processes, and a region of partial melt or a magma body can develop. These regions can themselves undergo physical processes that separate melt from crystals of the kind that have long been advocated for partial melt zones and magma chambers. Pure partial melt can be extracted to form pools of eruptible magma overlying a crystal-rich residuum.

DISCUSSION

An integrated model for generation of evolved igneous rocks at destructive plate margins is proposed. A combination of fluid-fluxed melting and decompression melting in the mantle wedge above subduction zones produces basaltic magmas with a wide range of compositions and H_2O contents, which ascend into the arc crust. Much of this magma is intruded into the deeper parts of the crust. Primitive basalts extracted directly from the

mantle only rarely reach the Earth's surface. Numerous incremental intrusions of basalt into the crust generate a deep crustal hot zone of accumulating magma, heat and volatiles. H_2O-rich intermediate to silicic residual melts are generated by incomplete crystallization of newly arrived basalt, with some contribution from remelting of earlier intrusions and partial melting of older crustal rocks induced by heat transfer and fluid fluxing from the crystallizing basalts. Involvement of older crust in the hot zone can account for the isotopic signatures of some arc rocks, especially at continental margins (Hildreth & Moorbath, 1988). As the hot zone evolves, gradients of temperature, pressure, H_2O content and melt fraction develop. In this way the hot zone can be a major cause of geochemical variation in arc magmas, from rhyolite at low melt fraction, through dacite to andesite at melt fractions of $\geq 0{\cdot}35$, to evolved arc basalts when the intrusion depth is sufficiently deep at the Moho or in the uppermost mantle. Residual melts derived from primitive hydrous basalt are H_2O-rich and therefore have low viscosities. Such melts have calculated segregation times in the range 10^3–10^6 years, but ascent times that are geologically instantaneous.

An important implication of our model is that the deep crust and upper mantle geotherm exerts the primary control on the compositions of melts. The geotherm is itself partly governed by influx of heat from intruding magmas as well as thermal conduction. In our models, focusing of intrusions at a given depth leads to the development of a thermal perturbation, which develops very slowly over millions of years. At any one time intrusions at different levels in the deep roots of the arc will cool to the local temperature, creating a variation in melt fraction and composition with depth from the most evolved, rhyolitic, melts generated at depths just below the 720°C solidus isotherm, to andesites and dacites at temperatures of 900–1050°C at greater depths, and to evolved basalts at 1050–1200°C. Our model results suggest that if magma intrusion is focused at a particular depth then melts will be generated within a narrow compositional spread, whereas if intrusions occur over a wide depth range there will be a corresponding wide range of melt compositions. In essence, the thicker the crust, the greater the potential diversity of residual melt compositions. There is also likelihood of multiple staging of magmas and more than one hot zone (Fig. 1). For example, evolved basalt magmas could be generated at Moho depths and then intruded into a higher level hot zone where more evolved magmas are generated. A corollary of our model is that once a hot zone is developed at depth, the likelihood of mantle-derived magmas passing through this zone without some degree of processing, however modest, is very low. Hot zones may in part account for the remarkable scarcity of mantle-derived magmas in mature volcanic arcs.

H_2O-rich magmas ascending from deep hot zones may entrain restite or cumulates from their source region and/or incorporate wall-rock during ascent. Such materials can become dissolved in the ascending superheated magmas, generating further compositional and textural diversity. Magmas will crystallize rapidly and extensively when they intersect their H_2O-saturated liquidus in the upper crust, as a consequence of degassing. This expectation is consistent with the remarkably short (decades or less) residence times that are emerging from studies of trace element zoning in phenocrysts (Zellmer *et al.*, 1999; Costa *et al.*, 2003; Morgan *et al.*, 2004). We propose that the principal textural features of arc rocks are determined during this stage of evolution through the complex interplay of decompresssion, nucleation and growth of crystals (Blundy & Cashman, 2001). The H_2O content recorded in melt inclusions reflects the magma H_2O content at the time of shallow crystallization, and not necessarily the amount of H_2O initially dissolved in the melt at the point of segregation from its source. The large increase in viscosity that accompanies degassing and crystallization of hydrous melts is a major factor in stalling of ascending magmas in the upper crust to form ephemeral magma chambers or plutons. In the latter case we distinguish between an early, rapid episode of decompression-driven crystallization (Blundy & Cashman, 2001), and a subsequent, slow, episode of cooling-driven *in situ* crystallization. If plutons or magma chambers are assembled incrementally (e.g. Glazner *et al.*, 2004), by numerous pulses of chemically similar magma, then the thermal evolution of any particular magma batch may be very complex.

Our model includes the ephemeral growth of voluminous upper crustal magma bodies, or 'proto-plutons', that may undergo further fractionation and myriad processes such as melt segregation from crystal mushes (Bachmann & Bergantz, 2004), wall-rock assimilation, repeated episodes of recharge and magma mixing, and convective processes that can lead to either zoned chambers or homogeneous chambers. Mount Mazama is a good case of the development of a voluminous ($\sim$50 km^3) magma body over a period of at least 23 kya prior to the climactic 7 ka caldera-forming explosive eruption (Bacon, 1983). In this case, the shallow silicic magma body appears to have grown incrementally by additions of both H_2O-rich (high-Sr) and hotter, H_2O-poor (low-Sr), andesite magmas. Chemical and petrological data (Bacon & Druitt, 1988; Druitt & Bacon, 1989) indicate that these andesite magmas ascended from greater depth; we suggest that they originated from basalt crystallization in the hot zone. Rhyodacitic residual melts were generated within the chamber by both decompression crystallization and heat exchange with the growing body of well-stirred silicic magma. The silicic magma evolved by repeated additions of andesite and heat loss to the wall-rocks,

including melting of early formed plutonic equivalents. The Soufrière Hills andesite magma chamber can also be interpreted as the amalgamation of many additions of andesite magma from greater depth over a time period of centuries (Harford & Sparks, 2002; Zellmer *et al.*, 2003*a*, 2003*b*). Proto-plutons can be thermally rejuvenated by another pulse of hotter magma from below. This appears to have occurred beneath the Soufrière Hills Volcano (Devine *et al.*, 1998; Murphy *et al.*, 2000; Couch *et al.*, 2001), and in the production of the voluminous Fish Canyon Tuff (Bachmann *et al.*, 2002).

Our model has implications for the origin of arc-related granites. Chappell & White (2001) explain the linear chemical trends and relatively low temperatures of intermediate granitoid magmas as the consequence of unmixing rhyolitic partial melt from restite. This concept is not easy to reconcile with the textures of many such granites where evidence that most crystals grew from melt is manifest (e.g. oscillatory zoning in plagioclase). We propose that the same observations will result when H_2O-rich melts ascending from a deep crustal hot zone entrain and dissolve their own restite. One of the enigmas of granite plutons is that they can commonly be mapped over hundreds or thousands of square kilometres as discrete plutons with distinct textural features. It is hard to understand how such distinctive textural characteristics can arise if crystallization was exclusively the result of slow cooling in a long-lived shallow magma body. We explain this fundamental characteristic of many granite plutons by invoking long-lived hydrous melt generation in the lower crust followed by rapid ascent and degassing-induced, near-closed system crystallization in the upper crust. Large granite plutons are thus the amalgamation of many similar magma batches emplaced in the upper crust over long periods of time.

Our model has implications for the timescales of magmatic processes beneath volcanic arcs. The various crustal processes described above will each have a very different characteristic duration. Thermal incubation of the hot zone requires 10^5–10^6 years, depending on the initial geotherm and the magma input rate. After thermal incubation, individual sills will crystallize from their intrusion temperature down to 800–1000°C on timescales of 10–10^3 years, depending on sill thickness (Fig. 19), during which time the residual melt will evolve to more silicic compositions. This is the timescale of magmatic differentiation from basalt to andesite. Differentiation will fractionate parent and daughter isotopes of the U-series and it is anticipated that U-series studies of cogenetic sequences of basalt and andesite will record the duration of sill cooling in the hot zone. If extraction of the residual melt is instantaneous then U-series data have the potential to constrain hot zone processes. Where melt segregation is delayed by slow porous media processes this timescale will be extended, melts and solid residues

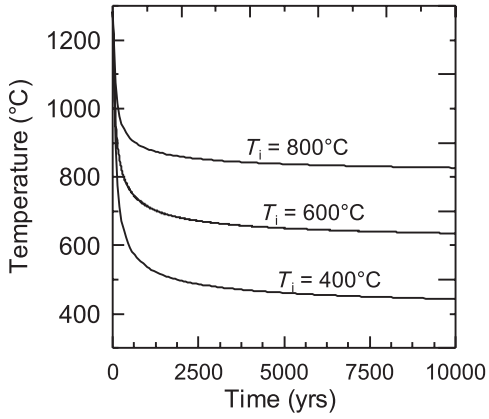

Fig. 19. Temperature vs time plot for conductive cooling of one 50 m basalt sill emplaced for different initial temperatures, T_i, of the country rocks. The basalt injection temperature is 1285°C and its H_2O content is 2·5 wt %. Different values of T_i correspond either to different levels on the geotherm or to different times in the overall evolution of the hot zone.

may continue to equilibrate, and the U-series picture may become extremely complicated. Berlo *et al.* (2004) have demonstrated that partial melting and crystallization processes in the deep crust are unable to generate significant excesses of ^{226}Ra over ^{230}Th. Thus, andesite magmas with ^{226}Ra excesses must have been generated from basaltic parents on a timescale of less than 8000 years. This is entirely consistent with our calculated sill cooling times (Fig. 19). In contrast, silicic arc magmas commonly show U–Th equilibria (Turner *et al.*, 2000) consistent with long residence times as partial melt in the hot zone, which we attribute to their higher viscosity and slower segregation.

Once magma has segregated from the hot zone, its ascent via dykes is expected to be rapid. The calculations in Table 2 suggest that transport from the deep crust to the point of H_2O saturation may take only a matter of days. No geochemical technique is able to resolve timescales this short, although rapid ascent may be recorded by earthquake swarms.

As the magma attains H_2O saturation it begins to crystallize. The timescale of crystallization of the phenocryst population (i.e. up to ~45% crystals) will be of the order of months to years (Table 2). In the absence of effective physical separation of crystals and melt this episode of crystallization will be very hard to date radiometrically. The situation will be further complicated by entrainment of older crystal populations (e.g. Cooper & Reid, 2003; Dungan & Davidson, 2004; Davidson *et al.*, 2005). However, because gas is continuously lost during crystallization, radiometric techniques that involve volatile components with short half-life isotopes, such as ^{222}Rn, ^{210}Pb and ^{210}Po, have the potential to date the timescales of decompression crystallization. Similarly, zoning of rapidly diffusing species in crystals (e.g.

Zellmer *et al.*, 1999; Costa *et al.*, 2003; Morgan *et al.*, 2004) is well suited to dating crystallization on these short timescales.

Once magma has become too viscous to continue its ascent, as a result of crystallization and H_2O loss, it will stall. Subsequent crystallization, up to the point of complete solidification, will occur over timescales controlled by slow thermal diffusion through the wall-rocks. Magma chambers and large plutons can grow in the shallow crust by incremental accumulation and amalgamation of rising batches of evolved magma; however, emerging evidence for geologically short residence and crystallization times suggests that development of upper crustal magma bodies occurs in pulses. This idea is consistent with the expectation that melt segregation processes from the hot zone will be pulsatory, geological evidence for well-defined plutonic contacts between intrusions, and emerging geochronological data that volcanoes have episodic pulses of high activity alternating with long periods of dormancy. Thermal rejuvenation of such proto-plutons by subsequent magma pulses will lead to extremely complicated radiometric data.

The model can apply to magmatism in other tectonic settings, such as rift zones, ocean island volcanoes and flood basalt provinces. The same principles can be applied with basalt intrusions in the deep crust generating differentiated residual melts or melting the crust. Annen & Sparks (2002) found that the relative amounts of crustal melt vs residual melt depend on the basalt temperature and volatile content together with the fertility of the crustal rocks. Cool, wet magmas (as occur in arcs and alkali basalt provinces) tend to generate large proportions of residual melt, whereas hot dry basalts (perhaps as in flood basalt provinces) tend to be very effective at remelting fertile crust but generate relatively little residual melt.

CONCLUSIONS

Fractional crystallization in shallow magma chambers and dehydration crustal melting are the current paradigms for generating intermediate to silicic magmas in arcs. In this study we propose that production of residual silicic melt by incomplete crystallization of wet basalt in a deep lower crustal hot zone, accompanied by volumetrically lesser melting of crustal rocks, is a more compelling concept. Our model is physically constrained by numerical simulation, supported by experimental petrology, and consistent with geophysical and petrological observations. We propose that production of H_2O-rich magmas with a wide diversity of chemical composition is a deep-seated process, controlled in detail by the geotherm.

Hydrous andesite magmas ascend and then stall in the upper crust where they undergo extensive crystallization induced first by degassing and subsequently by conductive cooling. The rate at which crystals nucleate and grow is a sensitive function of H_2O content and ascent path. Thus, whereas chemical diversity is primarily acquired at depth, textural diversity is acquired at shallow level. This explains why many granite plutons appear to have grown over long periods, by amalgamation of sequential batches of compositionally similar magma with distinctive textural characteristics that can be mapped in the field.

Of course, nature is much more complex than can be described by a simplified model and we acknowledge that many plutons or volcanoes require the involvement of shallow crustal processes to explain fully their petrography and geochemistry. Such processes include further fractionation of andesite magmas in zoned magma chambers, magma mingling, reheating of partially solidified proto-plutons, assimilation of shallow crustal wall-rocks and expulsion of evolved residual melts by filter pressing. We contend that these processes are superimposed upon the key process of melt generation in deep crustal hot zones.

ACKNOWLEDGEMENTS

The three authors have made equal contributions to this paper. B. Chappell kindly compiled the Cascades volcanic rock database used to construct Fig. 2. B. Scaillet kindly provided unpublished plagioclase composition data for Mount Pinatubo. We thank S. Powell for drafting Fig. 1. We are grateful to A. T. Anderson for useful discussions, and to anonymous referees of previous versions of the manuscript for an interesting debate that helped us to clarify our ideas. The paper benefited from the helpful reviews of J. Davidson, J. Dufek, A. Glazner, M. Pichavant and M. Reagan, as well as from the careful editorial handling of M. Wilson. C.A. was supported by a Swiss National Science Foundation Fellowship (8220-064666) and by a grant from the Ernst and Lucie Schmidheiny foundation. J.D.B. acknowledges a NERC Senior Research Fellowship. R.S.J.S. acknowledges a NERC Professorship and Royal Society–Wolfson Award.

REFERENCES

Allen, J. C. & Boettcher, A. L. (1983). The stability of amphibole in andesite and basalt at high-pressures. *American Mineralogist* **68**, 307–314.

Anderson, A. T. (1979). Water in some hypersthenic magmas. *Journal of Geology* **87**, 509–531.

Anderson, J. L. & Smith, D. R. (1995). The effects of temperature and fO_2 on the Al-in-hornblende barometer. *American Mineralogist* **80**, 549–559.

Annen, C. & Sparks, R. S. J. (2002). Effects of repetitive emplacement of basaltic intrusions on thermal evolution and melt generation in the crust. *Earth and Planetary Science Letters* **203**, 937–955.

Arculus, R. J. & Wills, K. J. A. (1980). The petrology of plutonic blocks and inclusions from the Lesser Antilles island arc. *Journal of Petrology* **21**, 743–799.

Atherton, M. P. & Petford, N. (1993). Generation of sodium-rich magmas from newly underplated basaltic crust. *Nature* **362**, 144–146.

Bachmann, O. & Bergantz, G. W. (2004). On the origin of crystal-poor rhyolites: extracted from batholithic crystal mushes. *Journal of Petrology* **45**, 1565–1582.

Bachmann, O. & Dungan, M. A. (2002). Temperature-induced Al-zoning in hornblendes of the Fish Canyon magma, Colorado. *American Mineralogist* **87**, 1062–1076.

Bachmann, O., Dungan, M. A. & Lipman, P. W. (2002). The Fish Canyon magma body, San Juan volcanic field, Colorado: rejuvenation and eruption of an upper-crustal batholith. *Journal of Petrology* **43**, 1469–1503.

Bacon, C. R. (1983). Eruptive history of Mount Mazama and Crater Lake Caldera, Cascade Range, USA. *Journal of Volcanology and Geothermal Research* **18**, 57–115.

Bacon, C. R. & Druitt, T. H. (1988). Compositional evolution of the zoned calcalkaline magma chamber of Mount Mazama, Crater Lake, Oregon. *Contributions to Mineralogy and Petrology* **98**, 224–256.

Bacon, C. R., Bruggman, P. E., Christiansen, R. L., Clynne, M. A., Donnelly-Nolan, J. M. & Hildreth, W. (1997). Primitive magmas at five Cascade volcanic fields: melts from hot, heterogeneous sub-arc mantle. *Canadian Mineralogist* **35**, 397–423.

Baker, D. R. (1998). Granitic melt viscosity and dike formation. *Journal of Structural Geology* **20**, 1395–1404.

Baker, M. B., Grove, T. L. & Price, R. (1994). Primitive basalts and andesites from the Mt Shasta region, N California—products of varying melt fraction and water-content. *Contributions to Mineralogy and Petrology* **118**, 111–129.

Barclay, J. & Carmichael, I. S. E. (2004). A hornblende basalt from western Mexico: water-saturated phase relations constrain a pressure–temperature window of eruptibility. *Journal of Petrology* **45**, 485–506.

Barclay, J., Rutherford, M. J., Carroll, M. J., Murphy, M. D., Devine, J. D., Gardner, J. & Sparks, R. S. J. (1998). Experimental phase equilibria constraints on pre-eruptive storage conditions of the Soufrière Hills magma. *Geophysical Research Letters* **25**, 3437–3440.

Bergantz, G. (1989). Underplating and partial melting: implications for melt generation and extraction. *Science* **245**, 1093–1095.

Berlo, K., Turner, S., Blundy, J. & Hawkesworth, C. (2004). The extent of U-series disequilibria produced during partial melting of the lower crust with implications for the formation of the Mount St. Helens dacites. *Contributions to Mineralogy and Petrology* **148**, 122–130.

Blatter, D. L. & Carmichael, I. S. E. (1998). Plagioclase-free andesites from Ziticuaro (Michoacan), Mexico: petrology and experimental constraints. *Contributions to Mineralogy and Petrology* **132**, 121–138.

Blatter, D. L. & Carmichael, I. S. E. (2001). Hydrous phase equilibria of a Mexican high-silica andesite: a candidate for a mantle origin? *Geochimica et Cosmochimica Acta* **65**, 4043–4065.

Blundy, J. & Cashman, K. (2001). Ascent-driven crystallisation of dacite magmas at Mount St Helens, 1980–1986. *Contributions to Mineralogy and Petrology* **140**, 631–650.

Blundy, J. & Cashman, K. (2005). Rapid decompression-driven crystallisation recorded by melt inclusions from Mount St. Helens volcano. *Geology* **33**, 793–796.

Bohrson, W. A. & Spera, F. J. (2001). Energy-constrained open system magmatic processes II: Application of energy-constrained assimilation–fractional crystallisation (EC-AFC) model to magmatic systems. *Journal of Petrology* **42**, 1019–1041.

Bons, P. D., Arnold, J., Elburg, M. A., Kalda, J., Soesoo, A. & van Milligen, B. P. (2004). Melt extraction and accumulation from partially molten rocks. *Lithos* **78**, 25–42.

Brasse, H., Lezaeta, P., Rath, V., Schwalenberg, K., Soyer, W. & Haak, V. (2002). The Bolivian Altiplano conductivity anomaly, *Journal of Geophysical Research* **107**, article number 2096.

Carmichael, I. S. E. (2002). The andesite aqueduct: perspectives on the evolution of intermediate magmatism in west–central (105–99°W) Mexico. *Contributions to Mineralogy and Petrology* **143**, 641–663.

Carmichael, I. S. E. (2004). The activity of silica, water, and the equilibration of intermediate and silicic magmas. *American Mineralogist* **89**, 1438–1446.

Carrigan, C. R. (1988). Biot-number and thermos bottle effect—implications for magma-chamber convection. *Geology* **16**, 771–774.

Carroll, M. R. & Wyllie, P. J. (1990). The system tonalite–H_2O at 15 kbar and the genesis of calc-alkaline magmas. *American Mineralogist* **75**, 345–357.

Cervantes, P. & Wallace, P. J. (2003). Role of H_2O in subduction-zone magmatism: new insights from melt inclusions in high-Mg basalts from central Mexico. *Geology* **31**, 235–238.

Chapman, D. S. & Furlong, K. P. (1992). Thermal state of the continental lower crust. In: Fountain, D. M., Arculus, R. & Kay, R. W. (eds) *Continental Lower Crust. Developments in Geotectonics* **23**, 179–199.

Chappell, B. W. & White, J. R. (2001). Two contrasting granite types: 25 years later: *Australian Journal of Earth Sciences* **48**, 489–499.

Chmielowski, J., Zandt, G. & Habeland, C. (1999). The Central Andean Altiplano–Puna magma body. *Geophysical Research Letters* **26**, 783–786.

Clemens, J. D. & Vielzeuf, D. (1987). Constraints on melting and magma production in the crust. *Earth and Planetary Science Letters* **86**, 287–306.

Clemens, J. D., Petford, N. & Mawer, C. K. (1997). Ascent mechanisms of granitic magmas: causes and consequences. In: Holness, M. B. (ed.) *Deformation-Enhanced Fluid Transport in the Earth's Crust and Mantle*. London: Chapman & Hall, pp. 145–172.

Clynne, M. A. (1999). A complex magma mixing origin for rocks erupted in 1915, Lassen Peak, California. *Journal of Petrology* **40**, 105–132.

Coleman, D. S., Gray, W. &. Glazner, A. F. (2004). Rethinking the emplacement and evolution of zoned plutons: geochronologic evidence for incremental assembly of the Tuolumne Intrusive Suite, California. *Geology* **32**, 433–436.

Conrey, R. M., Sherrod, D. R., Hooper, P. R. & Swanson, D. A. (1997). Diverse primitive magmas in the Cascade arc, northern Oregon and southern Washington. *Canadian Mineralogist* **35**, 367–396.

Cooper, K. M. & Reid, M. R. (2003). Re-examination of crystal ages in recent Mount St. Helens lavas: implications for magma reservoir processes. *Earth and Planetary Science Letters* **213**, 149–167.

Costa, F., Chakraborty, S. & Dohmen, R. (2003). Diffusion coupling between trace and major elements and a model for calculation of magma residence times using plagioclase. *Geochimica et Cosmochimica Acta* **67**, 2189–2200.

Costa, F., Scaillet, B. & Pichavant, M. (2004). Petrological and experimental constraints on the pre-eruption conditions of Holocene dacite from Volcan San Pedro (36°S, Chilean Andes) and the importance of sulphur in silicic subduction-related magmas. *Journal of Petrology* **45**, 855–881.

Cottrell, E., Gardner, J. E. & Rutherford, M. J. (1999). Petrologic and experimental evidence for the movement and heating of the pre-eruptive Minoan rhyodacite (Santorini, Greece). *Contributions to Mineralogy and Petrology* **135**, 315–331.

Couch, S., Sparks, R. S. J. & Carroll, M. R. (2001). Mineral disequilibrium in lava explained by convective self-mixing in open magma chambers. *Nature* **411**, 1037–1039.

Couch, S., Harford, C. L., Sparks, R. S. J. & Carroll, M. R. (2003). Experimental constraints on the conditions of formation of highly calcic plagioclase microlites at the Soufrière Hills Volcano, Montserrat. *Journal of Petrology* **44**, 1455–1475.

Crisp, J. (1984). Rates of magma emplacement and volcanic output. *Journal of Volcanology and Geothermal Research* **20**, 177–211.

Davidson, J. P., Tepley, F. J., III & Knesel, K. M. (1998). Crystal isotope stratigraphy; a method for constraining magma differentiation pathways. *EOS Transactions, American Geophysical Union* **79**, 185–189.

Davidson, J., Tepley, F., Palacz, Z. & Meffan-Main, S. (2001). Magma recharge, contamination and residence times revealed by *in situ* laser ablation isotopic analysis of feldspar in volcanic rocks. *Earth and Planetary Science Letters* **184**, 427–442.

Davidson, J. P., Hora, J. M. Garrison, J. M. & Dungan, M. A. (2005). Crustal forensics in arc magmas. *Journal of Volcanology and Geothermal Research* **140**, 157–170.

Davies, J. H. & Stevenson, D. J. (1992). Physical model of source region of subduction zone volcanics. *Journal of Geophysical Research* **97**, 2037–2070.

Debari, S. M. & Coleman, R. G. (1989). Examination of the deep levels of an island arc: evidence from the Tonsina ultramafic–mafic assemblage, Tonsina, Alaska. *Journal of Geophysical Research* **94**, 4373–4391.

De Bremond d'Ars, J., Jaupart, C. & Sparks, R. S. J. (1995). Distribution of volcanoes in active margins. *Journal of Geophysical Research* **100**, 20421–20432.

DePaolo, D. J. (1981). Trace-element and isotopic effects of combined wallrock assimilation and fractional crystallisation. *Earth and Planetary Science Letters* **53**, 189–202.

DePaolo, D. J., Perry, F. V. & Baldridge, W. S. (1992). Crustal versus mantle sources of granitic magmas—a 2-parameter model based on Nd isotopic studies. *Transactions of the Royal Society of Edinburgh, Earth Sciences* **83**, 439–446.

Devine, J. D., Murphy, M. D., Rutherford, M. J., Barclay, J., Sparks, R. S. J., Carroll, M. R., Young, S. R. & Gardner, J. E. (1998). Petrologic evidence for pre-eruptive pressure–temperature conditions, and recent re-heating, of andesite magma at Soufrière Hills Volcano, Montserrat, W.I. *Geophysical Research Letters* **25**, 3669–3672.

Devine, J. D., Rutherford, M. J., Norton, G. E. & Young, S. R. (2003). Magma storage region processes inferred from geochemistry of Fe–Ti oxides in andesitic magma, Soufrière Hills Volcano, Montserrat, WI. *Journal of Petrology* **44**, 1375–1400.

Dingwell, D. B., Hess, K. U. & Romano, C. (1998). Viscosity data for hydrous peraluminous granitic melts: comparison with a meta-luminous model. *American Mineralogist* **83**, 236–239.

Druitt, T. H. & Bacon, C. R. (1989). Petrology of the zoned calcalkaline magma chamber of Mount Mazama, Crater Lake, Oregon. *Contributions to Mineralogy and Petrology* **101**, 245–259.

Druitt, T. H., Edwards, L., Mellors, R. M., Pyle, D. M., Sparks, R. S. J., Lanphere, M., Davies, M. & Barriero, B. (eds) (1999). *Santorini Volcano. Geological Society, London, Memoirs* **19**.

Ducea, M. N. (2002). Constraints on the bulk composition and root foundering rates of continental arcs: a California arc perspective. *Journal of Geophysical Research* **107**, doi: 10.1029/2001JB000643.

Ducea, M. N. & Saleeby, J. B. (1996). Buoyancy sources for a large, unrooted mountain range, the Sierra Nevada, California: evidence from xenolith thermobarometry. *Journal of Geophysical Research* **101**, 8229–8244.

Ducea, M. N. & Saleeby, J. B. (1998*a*). A case for delamination of the deep batholithic crust beneath the Sierra Nevada, California. *International Geology Review* **40**, 78–93.

Ducea, M. N & Saleeby, J. B. (1998*b*). Crustal recycling beneath continental arcs: silica-rich glass inclusions in ultramafic xenoliths from the Sierra Nevada, California. *Earth and Planetary Science Letters* **156**, 101–116.

Dungan, M. A. & Davidson, J. (2004). Partial assimilative recycling of the mafic plutonic roots of arc volcanoes: an example from the Chilean Andes. *Geology* **32**, 773–776.

Eggler, D. H. (1972). Amphibole stability in H_2O-undersaturated calc-alkaline melts. *Earth and Planetary Science Letters* **15**, 38–44.

Eggler, D. H. & Burnham, C. W. (1973). Crystallisation and fractionation trends in the system andesite–H_2O–CO_2–O_2 at pressure to 10 Kbar *Geological Society of America Bulletin* **84**, 2517–2532.

Elkins-Tanton, L. T., Grove, T. L. & Donnelly-Nolan, J. (2001). Hot shallow melting under the Cascades volcanic arc. *Geology* **29**, 631–634.

Falloon, T. J. & Danyushevsky, L. V. (2000). Melting of refractory mantle at 1·5, 2 and 2·5 GPa under anhydrous and H_2O-undersaturated conditions: implications for the petrogenesis of high-Ca boninites and the influence of subduction components on mantle melting. *Journal of Petrology* **41**, 257–283.

Farmer, G. L., Glazner, A. F. & Manley, C. R. (2002). Did lithospheric delamination trigger late Cenozoic potassic volcanism in the southern Sierra Nevada, California? *Geological Society of America Bulletin* **114**, 754–768.

Feeley, T. C. & Davidson, J. P. (1994). Petrology of calc-alkaline lavas at Volcán Ollague and the origin of compositional diversity at Central Andean stratovolcanoes. *Journal of Petrology* **35**, 1295–1340.

Feeley, T. C. & Hacker, M. D. (1995). Intracrustal derivation of Na-rich andesitic and dacitic magmas—an example from Volcán Ollague, Andean Central Volcanic Zone. *Journal of Geology* **103**, 213–225.

Ferrara, G., Petrini, R., Serri, G. & Tonarini, S. (1989). Petrology and isotope-geochemistry of San-Vincenzo rhyolites (Tuscany, Italy). *Bulletin of Volcanology* **51**, 379–388.

Fliedner, M. M. & Klemperer, S. L. (2000). Crustal transition from oceanic arc to continental arc, eastern Aleutian Islands and Alaska Peninsula. *Earth and Planetary Science Letters* **179**, 567–579.

Fliedner, M. M., Ruppert, S. & SSCD Working Group (1996). Three-dimensional crustal structure of the southern Sierra Nevada from seismic fan profiles and gravity modeling. *Geology* **24**, 367–370.

Fliedner, M., Klemperer, S. L. & Christensen, N. I. (2000). Three-dimensional model of the Sierra Nevada arc, California, and its implications for crustal and upper mantle composition. *Journal of Geophysical Research* **105**, 10899–10921.

Foden, J. D. & Green, D. H. (1992). Possible role of amphibole in the origin of andesite: some experimental and natural evidence. *Contributions to Mineralogy and Petrology* **109**, 479–493.

Forneris, J. F. & Holloway, J. R. (2003). Phase equilibria in subducting basaltic crust: implications for H_2O release from the slab. *Earth and Planetary Science Letters* **214**, 187–201.

Gill, J. (1981). *Orogenic Andesites and Plate Tectonics*. Berlin: Springer, 390 pp.

Glazner, A. F. (1994). Foundering of mafic plutons and density stratification of continental crust. *Geology* **22**, 435–438.

Glazner, A. F., Bartley, J. M., Coleman, D. S., Gray, W. & Taylor, Z. T. (2004). Are plutons assembled over millions of years by amalgamation from small magma chambers? *GSA Today* **14**, 4–11.

Green, T. H. (1972). Crystallisation of calc-alkaline andesite under controlled high-pressure hydrous conditions. *Contributions to Mineralogy and Petrology* **34**, 150–166.

Green, T. H. (1982). Anatexis of mafic crust and high pressure crystallisation of andesite. In: Thorpe, R. S. (ed.) *Andesites: Orogenic Andesites and Related Rocks*. Chichester: John Wiley, pp. 465–487.

Green, T. H. (1992). Experimental phase equilibrium studies of garnet-bearing I-type volcanics and high-level intrusives from Northland, New Zealand. *Transactions of the Royal Society of Edinburgh, Earth Sciences* **83**, 429–438.

Green, T. H. & Pearson, N. J. (1985). Rare earth element partitioning between clinopyroxene and silicate liquid at moderate to high pressure. *Contributions to Mineralogy and Petrology* **91**, 24–36.

Grove, T. L. & Kinzler, R. J. (1986). Petrogenesis of andesites. *Annual Review of Earth and Planetary Sciences* **14**, 417–454.

Grove, T. L., Kinzler, R. J., Baker, M. B., Donnelly-Nolan, J. M. & Lesher, C. E. (1988). Assimilation of granite by basaltic magma at Burnt Lava Flow, Medicine Lake Volcano, Northern California—decoupling of heat and mass-transfer. *Contributions to Mineralogy and Petrology* **99**, 320–343.

Grove, T. L., Donnelly-Nolan, J. M. & Housh, T. (1997). Magmatic processes that generated the rhyolite of Glass Mountain, Medicine Lake volcano, N California. *Contributions to Mineralogy and Petrologyy* **127**, 205–223.

Grove, T. L., Parman, S. W., Bowring, S. A., Price, R. C. & Baker, M. B. (2002). The role of an H_2O-rich fluid component in the generation of primitive basaltic andesites and andesites from Mt. Shasta region, N California. *Contributions to Mineralogy and Petrology* **142**, 375–396.

Grove, T. L., Elkins-Tanton, L. T., Parman, S. W., Chatterjee, N., Müntener, O. & Gaetani, G. A. (2003). Fractional crystallisation and mantle-melting controls on calc-alkaline differentiation trends. *Contributions to Mineralogy and Petrology* **145**, 515–533.

Hammarstrom, J. M. & Zen, E-An (1986). Aluminum in hornblende: an empirical igneous geobarometer. *American Mineralogist* **71**, 1297–1313.

Hammer, J. A. & Rutherford, M. J. (2002). An experimental study of the kinetics of decompression-induced crystallisation in silicic melt. *Journal of Geophysical Research* **107**, 1–24.

Harford, C. L. & Sparks, R. S. J. (2001). Recent remobilisation of shallow-level intrusions on Montserrat revealed by hydrogen isotope composition of amphiboles. *Earth and Planetary Science Letters* **185**, 285–297.

Harford, C. L., Pringle, M. S., Sparks, R. S. J. & Young, S. R. (2002). The volcanic evolution of Montserrat using $^{40}Ar/^{39}Ar$ geochronology. In: Druitt, T. H. & Kokelaar, B. P. (eds) *The Eruption of Soufrière Hills Volcano, Montserrat, from 1995 to 1999. Geological Society, London, Memoirs* **21**, 93–113.

Hasegawa, A. & Nakajima, J. (2004). Geophysical constraints on slab subduction and arc magmatism. In: Sparks, R. S. J. & Hawkesworth, C. J. (eds) *The State of the Planet: Frontiers and Challenges in Geophysics*. Washington, DC: American Geophysical Union, pp. 81–94.

Heath, E., Turner, S. P., Macdonald, R., Hawkesworth, C. J. & van Calsteren, P. (1998). Long magma residence times at an island are volcano (Soufrière, St. Vincent) in the Lesser Antilles: evidence from U-238–Th-230 isochron dating. *Earth and Planetary Science Letters* **160**, 49–63.

Heiken, G. & Eichelberger, J. C. (1980). Eruptions at Chaos Crags, Lassen Volcanic National Park, California. *Journal of Volcanology and Geothermal Research* **7**, 443–481.

Higgins, M. D. & Roberge, J. (2003). Crystal size distribution of plagioclase and amphibole from Soufrière Hills volcano, Montserrat: evidence for dynamic crystallization–textural coarsening cycles. *Journal of Petrology* **44**, 1401–1411.

Hildreth, W. (1981). Gradients in silicic magma chambers: implications for lithospheric magmatism. *Journal of Geophysical Research* **86**, 10153–10192.

Hildreth, W. & Moorbath, S. (1988). Crustal contribution to arc magmatism in the Andes of Central Chile. *Contributions to Mineralogy and Petrology* **98**, 455–489.

Hirose, K. (1997). Melting experiments on lherzolite KLB-1 under hydrous conditions and generation of high-magnesian andesitic melts. *Geology* **25**, 42–44.

Holbrook, W. S., Mooney, W. D. & Christensen, N. I. (1992). The seismic velocity structure of the deep continental crust. In: Fountain, D. M., Arculus, R. & Kay, R. W. (eds) *Continental Lower Crust*. Amsterdam: Elsevier, pp. 1–43.

Hollister, L. S., Grissom, G. C., Peters, E. K., Stowell, H. H. & Sisson, V. B. (1987). Confirmation of the empirical correlation of Al in hornblende with pressure of solidification of calc-alkaline plutons. *American Mineralogist* **72**, 231–239.

Holtz, F. & Johannes, W. (1994). Maximum and minimum water content of granitic melts—implications for chemical and physical properties of ascending magmas. *Lithos* **32**, 149–159.

Huppert, H. E. & Sparks, S. J. (1988). The generation of granitic magma by intrusion of basalt into continental crust. *Journal of Petrology* **29**, 599–624.

Izebekov, P., Gardner, J. E. & Eichelberger, J. C. (2004). Comagmatic granophrye and dacite from Karymsky volcanic center, Kamchakta; experimental constraints and magma storage conditions. *Journal of Volcanology and Geothermal Research* **131**, 1–18.

Jackson, M. D., Cheadle, M. J. & Atherton, M. P. (2003). Quantitative modeling of granitic melt generation and segregation in the continental crust. *Journal of Geophysical Research* **108**, article number 2332.

Johannes, W. & Holtz, F. (1990). Formation and composition of H_2O-undersaturated granitic melts. In: Ashworth, J. R. & Brown, M. (eds) *High Temperature Metamorphism and Crustal Anatexis*. London: Unwin Hyman, pp. 87–104.

Johannes, W. & Koepke, J. (2001). Incomplete reaction of plagioclase in experimental dehydration melting of amphibolite. *Australian Journal of Earth Sciences* **48**, 581–590.

John, B. E. & Blundy, J. D. (1993). Emplacement-related deformation of granitoid magmas, Southern Adamello Massif, Italy. *Geological Society of America Bulletin* **105**, 1517–1541.

Jull, M. & Kelemen, P. B. (2001). On the conditions for lower crustal convective instability. *Journal of Geophysical Research* **106**, 6423–6446.

Kaszuba, J. P. & Wentland, R. F. (2000). Effect of carbon dioxide on dehydration melting reactions and melt compositions in the lower crust and the origin of alkaline rocks. *Journal of Petrology* **41**, 363–386.

Katsumata, A. & Kamaya, N. (2003). Low-frequency continuous tremor around the Moho discontinuity away from volcanoes in the south-west Japan. *Geophysical Research Letters* **30** (1020), doi: 10.1029, 2002.

Kay, R. W. & Kay, S. M. (1993). Delamination and delamination magmatism. *Tectonophysics* **219**, 177–189.

Kay, R. W., Kay, S. M & Arculus, R. J. (1992). Magma genesis and crustal processing. In: Fountain, D. M., Arculus, R. & Kay, R. W. (eds) *Continental Lower Crust*. Amsterdam: Elsevier, pp. 423–445.

Kawamoto, T. (1996). Experimental constraints on differentiation and H_2O abundance of calc-alkaline magmas. *Earth and Planetary Science Letters* **144**, 577–589.

Lister, J. R. & Kerr, R. C. (1991). Fluid-mechanical models of crack propagation and their application to magma transport in dykes. *Journal of Geophysical Research* **96**, 10049–10077.

Liu, J., Bohlen, S. R. & Ernst, W. G. (1996). Stability of hydrous phases in subducting oceanic crust. *Earth and Planetary Science Letters* **143**, 161–171.

Luhr, J. F. (1990). Experimental phase-relations of water-saturated and sulfur-saturated arc magmas and the 1982 eruptions of El Chichon Volcano. *Journal of Petrology* **31**, 1071–1114.

Maksimov, A. P., Kadik, A. A., Korovushkina, E. Y. & Akimoto, S. (1978). Crystallisation of an andesite melt with a fixed water content at pressures up to 12 kbar. *Geochemistry International* **15**, 20–29.

Marsh, B. D. (1981). On the crystallinity, probability of occurrence, and rheology of lava and magma. *Contributions to Mineralogy and Petrology* **78**, 85–98.

Martel, C., Pichavant, M., Holtz, F., Scaillet, B., Bourdier, J.-L. & Traineau, H. (1999). Effects of f_{O2} and H_2O on andesite phase relations between 2 and 4 kbar. *Journal of Geophysical Research* **104**, 29453–29470.

Mastin, L. G. & Ghiorso, M. S. (2001). Adiabatic temperature changes of magma–gas mixtures during ascent and eruption. *Contributions to Mineralogy and Petrology* **141**, 307–321.

McKenzie, D. (1985). The extraction of magma from the crust and mantle. *Earth and Planetary Science Letters* **74**, 81–91.

Menand, T. & Tait, S. R. (2002). The propagation of a buoyant liquid-filled fissure from a source under constant pressure: an experimental approach. *Journal of Geophysical Research* **107**, doi:10.1029/2001JB000589.

Montel, J.-M. & Vielzeuf, D. (1997). Partial melting of metagreywacke, Part II. Compositions of minerals and melts. *Contributions to Mineralogy and Petrology* **128**, 176–196.

Moore, G. & Carmichael, I. S. E. (1998). The hydrous phase equilibria (to 3 kbar) of an andesite and basaltic andesite from western Mexico: constraints on water content and conditions of phenocryst growth. *Contributions to Mineralogy and Petrology* **130**, 304–319.

Morgan, D. J., Blake, S., Rogers, N. W., DeVivo, B., Rolandi, G., Macdonald, R. & Hawkesworth, C. J. (2004). Time scales of crystal residence and magma chamber volume from modelling of diffusion profiles in phenocrysts: Vesuvius 1944. *Earth and Planetary Science Letters* **222**, 933–946.

Mortazavi, M. & Sparks, R. S. J. (2004). Origin of rhyolite and rhyodacite lavas and associated mafic inclusions of Cape Akrotiri, Santorini: the role of wet basalt in generating calcalkaline silicic magmas. *Contributions to Mineralogy and Petrology* **146**, 397–413.

Müntener, O., Kelemen, P. B. & Grove, T. L. (2001). The role of H_2O during crystallisation of primitive arc magmas under uppermost mantle conditions and genesis of igneous pyroxenites: an experimental study. *Contributions to Mineralogy and Petrology* **141**, 643–658.

Murphy, M. D., Sparks, R. S. J., Barclay, J., Carroll, M. R. & Brewer, T. S. (2000). Remobilization of andesite magma by intrusion of mafic magma at the Soufrière Hills Volcano, Montserrat West Indies. *Journal of Petrology* **41**, 21–42.

Musselwhite, D. S., De Paolo, D. J. & McCurry, M. (1989). The evolution of a silicic magma system—isotopic and chemical evidence from the Woods Mountains Volcanic Center, Eastern California. *Contributions to Mineralogy and Petrology* **101**, 19–29.

Navon, O. & Lyakhovsky, V. (1998). Vesiculation processes in silicic magmas. In: Gilbert, J. S. & Sparks, R. S. J. (eds) *The Physics of Explosive Volcanic Eruptions. Geological Society, London, Special Publications* **145**, 27–50.

Newman, S. & Lowenstern, J. B. (2002). VOLATILECALC: a silicate melt–H_2O–CO_2 solution model written in Visual Basic for Excel. *Computers and Geosciences* **28**, 597–604.

Nicholls, I. A. (1971). Petrology of Santorini Volcano, Cyclades, Greece. *Journal of Petrology* **12**, 67–119.

Nicholls, I. A. & Harris, K. L. (1980). Experimental rare earth element partition coefficient for garnet, clinopyroxene and amphibole coexisting with andesitic and basaltic liquids. *Geochimica et Cosmochimica Acta* **44**, 28–308.

Obara, K. (2002). Non-volcanic deep tremor associated with subduction in south-west Japan. *Science* **296**, 1679–1681.

Osborn, E. F. (1957). Role of oxygen pressure in the crystallisation and differentiation of basaltic magma. *American Journal of Science* **259**, 609–647.

Ozerov, A. Y. (2000). The evolution of high-alumina basalts of the Klyuchevskoy volcano, Kamchatka, Russia, based on microprobe analyses of mineral inclusions. *Journal of Volcanology and Geothermal Research* **95**, 65–79.

Parman, S. W. & Grove, T. L. (2004). Harzburgite melting with and without H_2O: experimental data and predictive modeling. *Journal of Geophysical Research* **109**(B02201), doi:10.1029/2003JB002566.

Patiño Douce, A. E. & Beard, J. S. (1996). Effect of P, $f(O_2)$ and Mg/Fe ratio on dehydration melting of model metagreywackes. *Journal of Petrology* **37**, 999–1024.

Petford, N. (2003). Rheology of granitic magmas during ascent and emplacement. *Annual Review of Earth and Planetary Sciences* **31**, 399–427.

Petford, N. & Atherton, M. (1996). Na-rich partial melts from newly underplated basaltic crust: the Cordillera Blanca Batholith, Peru. *Journal of Petrology* **37**, 1491–1521.

Petford, N. & Gallagher, K. (2001). Partial melting of mafic (amphibolitic) lower crust by periodic influx of basaltic magma. *Earth and Planetary Science Letters* **193**, 483–489.

Petford, N., Kerr, R. C. & Lister, J. R. (1993). Dike transport of granitoid magmas. *Geology* **21**, 845–848.

Petford, N., Cruden, A. R., McCaffrey, K. J. W. & Vigneresse, J.-L. (2000). Granite magma formation, transport and emplacement in the Earth's crust. *Nature* **408**, 669–673.

Pichavant, M., Mysen, B. O. & Macdonald, R. (2002*a*). Source and H_2O content of high-MgO magmas in island arc settings: an experimental study of a primitive calc-alkaline basalt from St. Vincent, Lesser Antilles arc. *Geochimica et Cosmochimica Acta* **66**, 2193–2209.

Pichavant, M., Martel, C., Bourdier, J. L. & Scaillet, B. (2002*b*). Physical conditions, structure, and dynamics of a zoned magma chamber: Mount Pelée (Martinique, Lesser Antilles Arc). *Journal of Geophysical Research* **107**, article number 2093.

Prouteau, G. & Scaillet, B. (2003). Experimental constraints on the origin of the 1991 Pinatubo dacite. *Journal of Petrology* **44**, 2203–2241.

Raia, F. & Spera, F. J. (1997). Simulation of the growth and differentiation of continental crust. *Journal of Geophysical Research* **102**, 22629–22648.

Rapp, R. P. (1995). Amphibole-out phase-boundary in partially melted metabasalt, its control over liquid fraction and composition, and source permeability. *Journal of Geophysical Research* **100**, 15601–15610.

Rapp, R. P. & Watson, E. B. (1995). Dehydration melting of metabasalt at 8–32 kbar—implications for continental growth and crust–mantle recycling. *Journal of Petrology* **36**, 891–931.

Reagan, M. K., Sims, K. W. W., Erich, J., Thomas, R. B., Cheng, H., Edwards, R. L., Layne, G. & Ball, L. (2003). Time-scales of differentiation from mafic parents to rhyolite in North American continental arcs. *Journal of Petrology* **44**, 1703–1726.

Reagan, M., Tepley, F. J., Gill, J. B., Wortel, W. & Hartman, B. (2005). Rapid time scales of basalt to andesite differentiation at Anatahan volcano, Mariana Islands. *Journal of Volcanology and Geothermal Research* **146**, 171–183.

Rogers, G. & Hawkesworth, C. J. (1989). A geochemical traverse across the North Chilean Andes—evidence for crust generation from the mantle wedge. *Earth and Planetary Science Letters* **91**, 271–285.

Rubin, A. M. (1995). Propagation of magma-filled cracks. *Annual Review of Earth and Planetary Sciences* **23**, 287–336.

Rudnick, R. L. & Fountain, D. M. (1995). Nature and composition of the continental crust: a lower crustal perspective. *Reviews of Geophysics* **33**, 267–309.

Rutherford, M. J. & Devine, J. D. (1988). The May 18, 1980, eruption of Mount St. Helens, 3. Stability and chemistry of amphibole in the magma chamber. *Journal of Geophysical Research* **93**, 11949–11959.

Rutherford, M. J. & Devine, J. D. (2003). Magmatic conditions and magma ascent as indicated by hornblende phase equilibria and reactions in the 1995–2002 Soufrière Hills magma. *Journal of Petrology* **44**, 1433–1454.

Rutherford, M. J. & Hill, P. M. (1993). Magma ascent rates from amphibole breakdown—an experimental study applied to the 1980–1986 Mount St. Helens eruptions. *Journal of Geophysical Research* **98**, 19667–19685.

Rutherford, M. J., Sigurdsson, H., Carey, S. & Davis, A. (1985). The May 18, 1980, eruption of Mount St Helens, 1. Melt composition and experimental phase-equilibria. *Journal of Geophysical Research* **90**, 2929–2947.

Sato, H., Nakada, S., Fujii, T., Nakamura, M. & Suzuki-Kamata, K. (1999). Groundmass pargasite in the 1991–1995 dacite of Unzen volcano: phase stability experiments and volcanological implications. *Journal of Volcanology and Geothermal Research* **89**, 197–212.

Scaillet, B. & Evans, B. W. (1999). The 15 June 1991 eruption of Mount Pinatubo. I. Phase equilibria and pre-eruption P–T–fO_2–fH_2O conditions of the dacite magma. *Journal of Petrology* **40**, 381–411.

Schmidt, M. W. & Poli, S. (1998). Experimentally based water budgets for dehydrating slabs and consequences for arc magma generation. *Earth and Planetary Science Letters* **163**, 361–379.

Sekine, T. & Aramaki, S. (1992). Physical conditions of felsic magma constrained by experimentally-determined phase relations. *Geochemical Journal* **26**, 279–290.

Sekine, T., Katsura, T. & Aramaki, S. (1979). Water saturated phase-relations of some andesites with application to the estimation of the initial temperature and water-pressure at the time of eruption. *Geochimica et Cosmochimica Acta* **43**, 1367–1376.

Sen, C. & Dunn, T. (1994). Dehydration melting of a basaltic composition amphibolite at 1·5 and 2·0 GPa—implications for the origin of adakites. *Contributions to Mineralogy and Petrology* **117**, 394–409.

Sisson, T. W. & Bacon, C. R. (1999). Gas-driven filter pressing in magmas. *Geology* **27**, 613–616.

Sisson, T. W. & Bronto, S. (1998). Evidence for pressure-release melting beneath magmatic arcs from basalt at Galunggung, Indonesia. *Nature* **391**, 883–886.

Sisson, T. W. & Grove, T. L. (1993). Experimental investigations of the role of H_2O in calc-alkaline differentiation and subduction zone magmatism. *Contributions to Mineralogy and Petrology* **113**, 143–166.

Sisson, T. W. & Layne, G. D. (1993). H_2O in basalt and basaltic andesite glass inclusions from four subduction-related volcanoes. *Earth and Planetary Science Letters* **117**, 619–635.

Sisson, T. W., Ratajeski, K., Hankins, W. B. & Glazner, A. F. (2005). Voluminous granitic magmas from common basaltic sources. *Contributions to Mineralogy and Petrology* **148**, 635–661.

Smith, D. R. & Leeman, W. P. (1987). Petrogenesis of Mount St. Helens dacitic magmas. *Journal of Geophysical Research* **92**, 10313–10334.

Smith, R. L. (1979). Ash-flow magmatism. *Geological Society of America, Special Papers* **180**, 5–27.

Stanley, W. D., Mooney, W. D. & Fuis, G. S. (1990). Deep crustal structure of the Cascade Range and surrounding regions from seismic refraction and magnetotelluric data. *Journal of Geophysical Research* **95**, 19419–19438.

Stasiuk, M. V., Jaupart, C. & Sparks, R. S. J. (1993). Variations of flow rate and volume during eruption of lava. *Earth and Planetary Science Letters* **114**, 505–516.

Stratford, W. R. & Stern, T. A. (2004). Strong seismic reflections and melts in the mantle of a continental back-arc basin. *Geophysical Research Letters* **31**, L06622.

Tait, S. R., Huppert, H. E. & Sparks, R. S. J. (1984). The role of compositional convection in the formation of adcumulate rocks. *Lithos* **17**, 139–146.

Tatsumi, Y. (1982). Origin of high-magnesian andesites in the Setouchi Volcanic Belt, Southwest Japan, 2. Melting phase-relations at high pressures. *Earth and Planetary Science Letters* **60**, 305–317.

Tatsumi, Y. & Eggins, S. (1995). *Subduction Zone Magmatism*. Oxford: Blackwell Scientific.

Tepper, J. H., Nelson, B. K., Bergantz, G. W. & Irving, A. J. (1993). Petrology of the Chiilwack batholith, North Cascades, Washington. Generation of calc-alkaline granitoids by melting of mafic lower crust with variable water fugacity. *Contributions to Mineralogy and Petrology* **113**, 333–351.

Turner, S., Bourdon, B., Hawkesworth, C. & Evans, P. (2000). ^{226}Ra–^{230}Th evidence for multiple dehydration events, rapid ascent and the time scales of differentiation beneath the Tonga–Kermadec island arc. *Earth and Planetary Science Letters* **179**, 581–593.

Ulmer, P. (2001). Partial melting in the mantle wedge—the role of H_2O in the genesis of mantle-derived 'arc-related' magmas. *Physics of the Earth and Planetary Interiors* **127**, 215–232.

Wallace, P. J. (2001). Volcanic SO_2 emissions and the abundance and distribution of exsolved gas in magma bodies. *Journal of Volcanology and Geothermal Research* **108**, 85–106.

Whitney, J. A. (1988). The origin of granite—the role and source of water in the evolution of granitic magmas. *Geological Society of America Bulletin* **100**, 1886–1897.

Wolf, M. B. & Wyllie, P. J. (1994). Dehydration melting of amphibolite at 10 kbar—the effects of temperature and time. *Contributions to Mineralogy and Petrology* **115**, 369–383.

Wood, B. J. (2004). Melting of fertile peridotite with variable amounts of H_2O. In: Sparks, R. S. J. & Hawkesworth, C. J. (eds) *The State of the Planet: Frontiers and Challenges in Geophysics*. Washington, DC: American Geophysical Union, pp. 69–80.

Wyborn, D., Chappell, B. W. & James, M. (2001). Examples of convective fractionation in high-temperature granites from the Lachlan Fold Belt. *Australian Journal of Earth Sciences* **48**, 531–541.

Yogodzinsky, G. M. & Kelemen, P. B. (1998). Slab melting in the Aleutians: implications of an ion probe study of clinopyroxene in primitive adakite and basalt. *Earth and Planetary Science Letters* **158**, 53–65.

Yuan, X., Sobolev, S. V. Kind, R., Oncken, O., Bock, G., Asoh, G., *et al.*, (2000). Subduction and collision processes in the Central Andes constrained by converted seismic phases. *Nature* **408**, 958–961.

Zandt, G., Gilbert, H., Owens, T. J., Ducea, M., Saleeby, J. & Jones, C. H. (2004). Active foundering of a continental arc root beneath the southern Sierra Nevada in California. *Nature* **431**, 41–46.

Zellmer, G. F., Blake, S., Vance, D., Hawkesworth, C. & Turner, S. (1999). Plagioclase residence times at two island arc volcanoes (Kameni islands, Santorini, and Soufrière, St. Vincent) determined by Sr diffusion systematics. *Contributions to Mineralogy and Petrology* **136**, 345–357.

Zellmer, G. F., Hawkesworth, C. J., Sparks, R. S. J., Thomas, L. E., Harford, C. L., Brewer, T. S. & Loughlin, S. C. (2003*a*).

Geochemical evolution of the Soufrière Hills volcano, Montserrat, Lesser Antilles volcanic arc. *Journal of Petrology* **44**, 1349–1374.

Zellmer, G. F., Sparks, R. S. J., Hawkesworth, C. J. & Wiedenbeck, M. (2003*b*). Magma emplacement and remobilisation timescales beneath Montserrat: insights from Sr and Ba zonation in plagioclase phenocrysts. *Journal of Petrology* **44**, 1349–1374.

Zhang, Y. X. (1999). H_2O in rhyolitic glasses and melts: measurement, speciation, solubility, and diffusion. *Reviews of Geophysics* **37**, 493–516.